Article

Cell

Ultraconserved Enhancers Are Required for Normal Development

Graphical Abstract

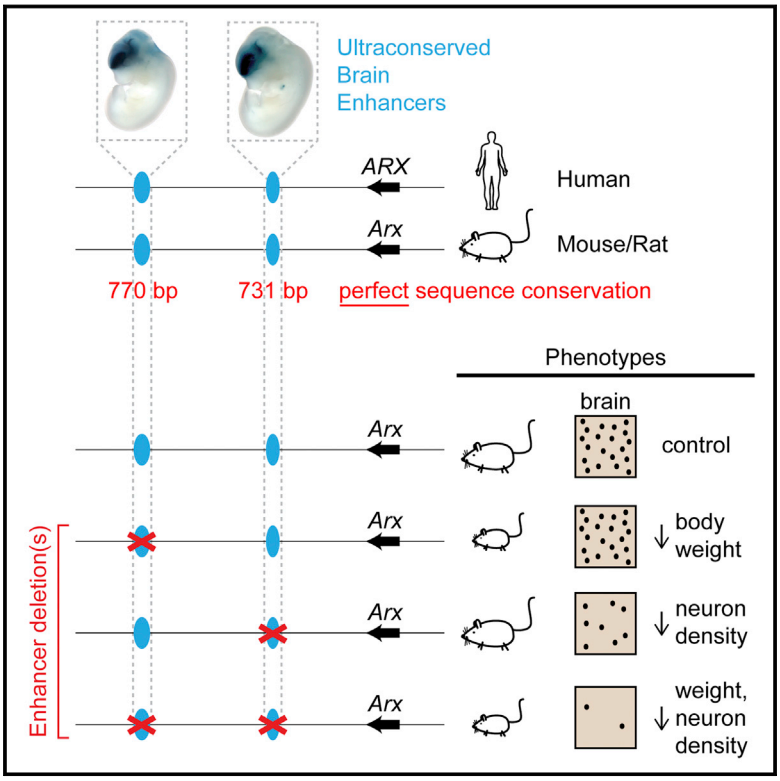

Highlights

- The *Arx* locus has a high density of very long ultraconserved forebrain enhancers
- Single or pairwise deletion of these enhancers results in viable mice in all cases
- In most cases, individual enhancer loss results in developmental anomalies
- Selection against these fitness deficits likely contributes to ultraconservation

Authors

Diane E. Dickel, Athena R. Ypsilanti, Ramón Pla, ..., John L.R. Rubenstein, Len A. Pennacchio, Axel Visel

Correspondence

dedickel@lbl.gov (D.E.D.), lapennacchio@lbl.gov (L.A.P.), avisel@lbl.gov (A.V.)

In Brief

Although initial studies suggested that loss of ultraconserved enhancers had no impact on viability, these sequences are now shown to be required for normal development.

Dickel et al., 2018, Cell *172*, 491–499
January 25, 2018
https://doi.org/10.1016/j.cell.2017.12.017

CellPress

Cell

Ultraconserved Enhancers Are Required for Normal Development

Diane E. Dickel,[1,*] Athena R. Ypsilanti,[2,6] Ramón Pla,[2,6] Yiwen Zhu,[1] Iros Barozzi,[1] Brandon J. Mannion,[1] Yupar S. Khin,[2] Yoko Fukuda-Yuzawa,[1] Ingrid Plajzer-Frick,[1] Catherine S. Pickle,[1] Elizabeth A. Lee,[1] Anne N. Harrington,[1] Quan T. Pham,[1] Tyler H. Garvin,[1] Momoe Kato,[1] Marco Osterwalder,[1] Jennifer A. Akiyama,[1] Veena Afzal,[1] John L.R. Rubenstein,[2] Len A. Pennacchio,[1,3,4,*] and Axel Visel[1,3,5,7,*]

[1]Environmental Genomics and Systems Biology Division, Lawrence Berkeley National Laboratory, 1 Cyclotron Road, Berkeley, CA 94720, USA

[2]Department of Psychiatry, Neuroscience Program, UCSF Weill Institute for Neurosciences and the Nina Ireland Laboratory of Developmental Neurobiology, University of California San Francisco, San Francisco, CA 94158, USA

[3]U.S. Department of Energy Joint Genome Institute, Walnut Creek, CA 94598, USA

[4]Comparative Biochemistry Program, University of California Berkeley, Berkeley, CA 94720, USA

[5]School of Natural Sciences, University of California Merced, Merced, CA 95343, USA

[6]These authors contributed equally

[7]Lead Contact

*Correspondence: dedickel@lbl.gov (D.E.D.), lapennacchio@lbl.gov (L.A.P.), avisel@lbl.gov (A.V.)

https://doi.org/10.1016/j.cell.2017.12.017

SUMMARY

Non-coding "ultraconserved" regions containing hundreds of consecutive bases of perfect sequence conservation across mammalian genomes can function as distant-acting enhancers. However, initial deletion studies in mice revealed that loss of such extraordinarily constrained sequences had no immediate impact on viability. Here, we show that ultraconserved enhancers are required for normal development. Focusing on some of the longest ultraconserved sites genome wide, located near the essential neuronal transcription factor *Arx*, we used genome editing to create an expanded series of knockout mice lacking individual or combinations of ultraconserved enhancers. Mice with single or pairwise deletions of ultraconserved enhancers were viable and fertile but in nearly all cases showed neurological or growth abnormalities, including substantial alterations of neuron populations and structural brain defects. Our results demonstrate the functional importance of ultraconserved enhancers and indicate that remarkably strong sequence conservation likely results from fitness deficits that appear subtle in a laboratory setting.

INTRODUCTION

One of the most astonishing observations from the sequencing of the human, mouse, and rat genomes was the finding of 481 loci of perfect sequence conservation between these species (minimum length 200 contiguous base pairs), despite the ~80 million years since their last common ancestor (Bejerano et al., 2004). Dubbed "ultraconserved" sequences, more than half of these sites display no evidence for protein-coding function. These noncoding elements are enriched near transcription factor genes expressed during embryogenesis (Bejerano et al., 2004; Sandelin et al., 2004), suggesting a possible role in regulating the expression of essential developmental genes. Indeed, we previously tested more than 200 noncoding ultraconserved sites using *in vivo* transgenic mouse reporter assays, which revealed that at least half act as transcriptional enhancers during embryonic development (Pennacchio et al., 2006; Visel et al., 2008).

Given their likely role in regulating the expression of vital genes, along with their extreme sequence conservation, noncoding ultraconserved elements were broadly assumed to be essential for life. However, the targeted deletion of four ultraconserved enhancers resulted in mice that were viable, fertile, and did not have any obviously detrimental phenotypes (Ahituv et al., 2007). This perplexing observation resulted in much speculation as to why these sites retained extreme sequence conservation in the apparent absence of deleterious effects, including hypotheses such as undetected subtle phenotypes selected against over longer time periods, functional redundancy of enhancers, or even atypical molecular functions (Ahituv et al., 2007; Chiang et al., 2008; McLean and Bejerano, 2008).

In the present study, we generated a series of mouse lines with single or pairwise deletions of ultraconserved enhancers to explore these possible explanations. We focused on a region on the X chromosome that contains the longest ultraconserved sites genome-wide (Bejerano et al., 2004). The region also encompasses the *Aristaless-related homeobox* (*ARX*/*Arx*) gene, mutations in which cause a variety of severe neurological phenotypes (Gécz et al., 2006; Kitamura et al., 2002). At least four of the ultraconserved sites within this region show enhancer activity in the developing forebrain that is similar to *Arx* gene expression (Pennacchio et al., 2006; Visel et al., 2013). We observed that nearly all single and pairwise enhancer deletions resulted in non-lethal, but identifiable abnormalities, including reduced growth and impaired brain development. Our results demonstrate that loss

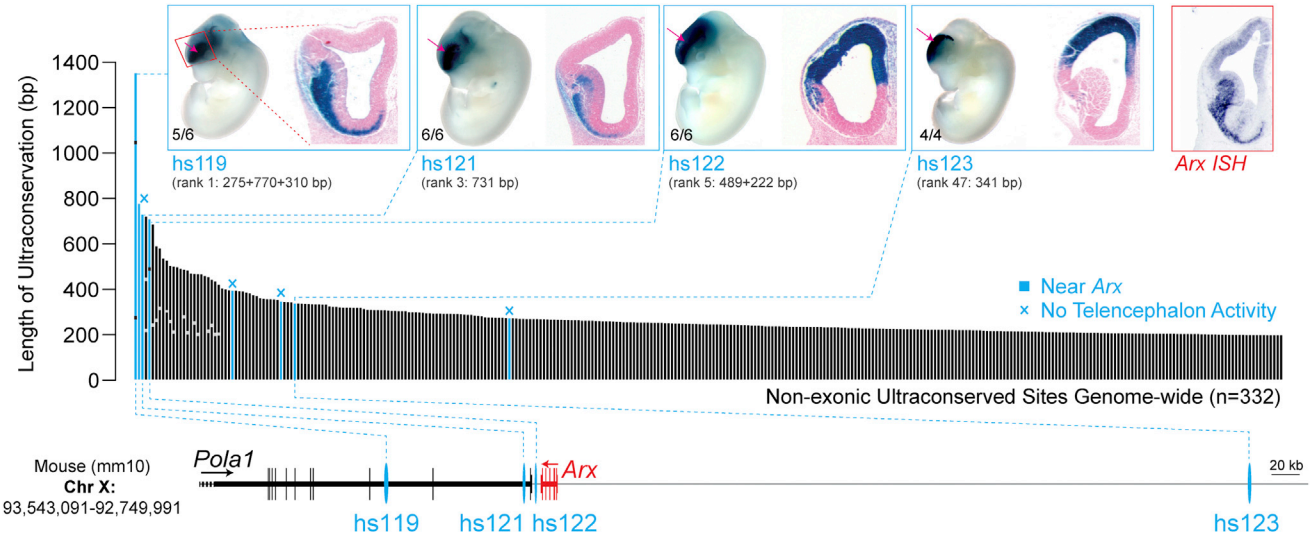

Figure 1. Selection of Ultraconserved Sites Examined

Bar graph shows the length of ultraconservation for all non-exonic human-rodent ultraconserved sites. Regions containing multiple sequences of perfect human-mouse-rat conservation ≥200 bp with <1 kb of intervening sequence were combined into a single ultraconserved site, with black or light gray tick marks indicating the length of the individual constitutive ultraconserved elements. Top: representative images showing the activity pattern (blue staining, pink arrows) of each telencephalon enhancer near *Arx* in an embryonic day 12.5 (E12.5) transgenic mouse embryo (left; Pennacchio et al., 2006) and specifically in the telencephalon in coronal forebrain sections (right; Visel et al., 2013). VISTA enhancer identifiers are indicated in blue text (hs numbers), and transgenic assay reproducibility is indicated in the bottom left corner of each panel. *Arx* is expressed in both the dorsal and ventral telencephalon at E12.5 (far right). *ISH*: *in situ* hybridization. Bottom: an overview of the *Arx* genomic locus, located on the X chromosome, showing the position of telencephalon enhancers selected for further study (blue ovals).

of ultraconserved enhancers, while broadly compatible with life, causes phenotypes that appear subtle in the laboratory but likely lead to decreased fitness over evolutionary time.

RESULTS

To examine the biological function of ultraconserved sequences beyond initial deletion studies (Ahituv et al., 2007), we focused on an 800 kb region of the X chromosome in which eight non-exonic ultraconserved sites are found, along with the *Arx* gene (Bejerano et al., 2004) (Figure 1). Each of the eight sites contains up to three adjacent ultraconserved elements of ≥200 bp of perfect conservation, and the locus harbors four of the five longest non-exonic ultraconserved sites in the human genome (Figure 1). We previously showed that five of the eight sites have transcriptional enhancer activity in the embryonic day 12.5 (E12.5) forebrain in transgenic mouse reporter assays, including four with highly reproducible activity in the telencephalon (Figure 1) and one with weakly reproducible activity in the diencephalon (Pennacchio et al., 2006).

Of the four telencephalon enhancers, two drive gene expression in similar regions of the ventral telencephalon, while the other two are active in similar dorsal domains, suggesting that pairs of enhancers at this locus may be active in the same cell types and potentially have redundant functions (Visel et al., 2013; Figure 1). Collectively, these dorsal and ventral telencephalon enhancer activity patterns are strikingly similar to the expression pattern of *Arx* (Visel et al., 2013; Figure 1), suggesting a regulatory interaction between these enhancers and this neighboring gene in the developing forebrain. Because of the high density of unusually long and possibly functionally redundant ultraconserved enhancers, this locus provides a testbed for assessing the role of ultraconserved enhancers in development. In particular, it is an ideal locus to assess possible explanations, such as enhancer redundancy or sub-lethal deleterious phenotypes, that were proposed to explain the initial observations that ultraconserved enhancers are not required for viability.

Ultraconserved Forebrain Enhancers Are Active in *Arx*-Expressing Cells

First, we sought to verify that these enhancers are active in *Arx*-expressing cells and to determine their cell-type specificity, because this information can be used to guide downstream phenotyping of enhancer deletion mice. We created a series of transgenic reporter mice, each with one of the ultraconserved telencephalon enhancers driving expression of a fluorescent reporter gene in the embryonic forebrain (see STAR Methods). We then performed single-cell RNA sequencing (RNA-seq) using Drop-Seq (Macosko et al., 2015), separately for each enhancer, on E12.5 whole forebrains from these embryos (Figure 2A; Table S1). Across all experiments, we reconstructed gene expression profiles for nearly 5,000 single cells (Figures 2B and S1A; Table S1). We masked the expression of the reporter gene and clustered the cells by gene expression similarity, which identified nine distinct cell types present, including two cell types that had robust expression of *Arx*. The first is a population of radial glia and neural progenitor cells, and the second is a cluster containing immature neurons,

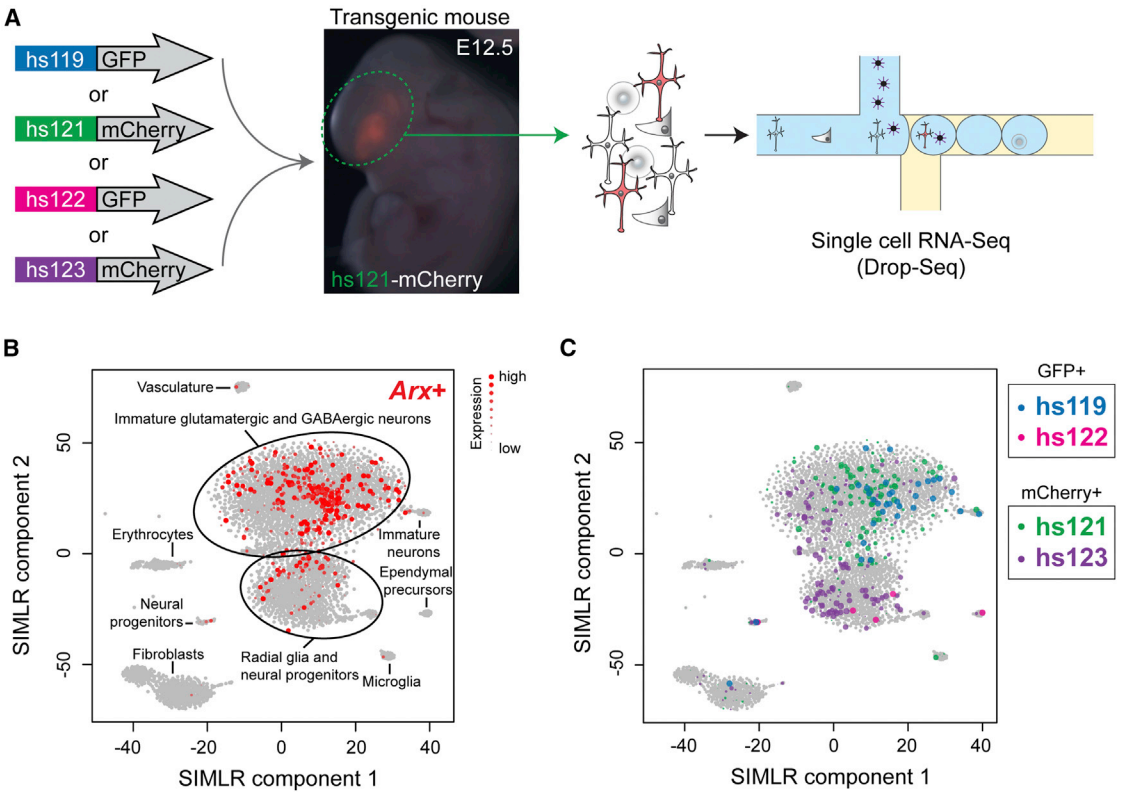

Figure 2. Ultraconserved Enhancers Near *Arx* Are Active in *Arx*-Expressing Cells

(A) To identify the specific cell type each enhancer is active in, we generated E12.5 transgenic embryos containing each one of the enhancers driving a fluorescent reporter gene and performed single-cell RNA-seq by Drop-seq on isolated forebrain tissue.

(B) Cumulative results of single-cell RNA-seq performed on E12.5 forebrain from all transgenic enhancer-reporter experiments. Each point indicates a unique single cell profiled (4,723 total), and cells were clustered by similarity of RNA expression. Red indicates cells where at least one *Arx* transcript was captured, and these points are scaled by decile of *Arx* expression, as shown in the legend.

(C) Same plot as (B), color-coded to indicate cells where one of the ultraconserved telencephalic enhancers drove reporter gene expression. Points indicating mCherry expression are scaled by expression level decile (larger points indicate higher expression).

See also Figure S1 and Tables S1 and S2.

including both GABAergic and glutamatergic types (Figure 2B; see also Figures S1A–S1C and Table S2 for relevant marker genes). We next examined which cells displayed expression of the reporter gene, which revealed that all four ultraconserved telencephalon enhancers drove reporter gene expression in at least one of these two *Arx*-expressing cell types (Figures 2C and S1D). Both ventral forebrain enhancers (hs119 and hs121) are active predominantly in the immature neuron cluster, particularly in neurons expressing GABAergic marker genes (Figures S1B and S1D), consistent with the known activity of hs121 in GABAergic neurons later in embryogenesis (Colasante et al., 2008). The dorsal enhancer hs123 is active predominantly in the radial glia/neural progenitor cells, with additional activity in immature neurons that have a glutamatergic identity (Figures S1C and S1D). Although few reporter-expressing cells were recovered for the dorsal enhancer hs122, the majority are radial glia/neural progenitor cells (Figure S1D). Together, these results support that the four ultraconserved enhancers collectively activate the expression of *Arx* in at least two different *Arx*-expressing cell populations.

Single- and Double-Knockout of Ultraconserved Enhancers Results in Viable Mice

To examine the *in vivo* function of these ultraconserved enhancers, we used CRISPR/Cas9 genome editing in fertilized eggs to generate a series of mouse lines, each missing one of the four enhancers (Figures 3A and S2; Table S3). This included one ultraconserved enhancer (hs121, also named UC467) whose deletion was previously reported to produce viable animals (Ahituv et al., 2007). Additionally, to examine the possibility of functional redundancy between ultraconserved enhancers limiting deleterious effects, we generated deletions of pairs of enhancers with similar activity patterns (both dorsal or both ventral) on the same haplotype (Figures 3A and S2; Table S3). In all cases, viable founder mice for each targeted deletion were obtained (Table S3). Taking advantage of the location of *Arx* on the X chromosome, we out-crossed correctly targeted founder mice to wild-type animals to obtain hemizygous null males for phenotyping. Male *Arx* gene knockout (hemizygous null) mice die within 2 days after birth and have severe developmental defects, including smaller brains and testicular and

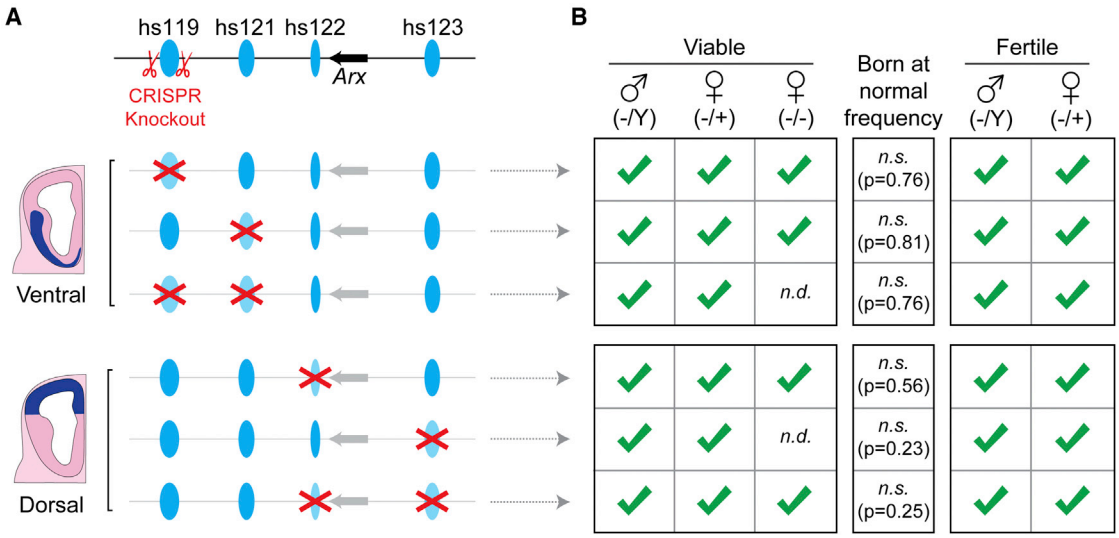

Figure 3. Single and Pairwise Deletion of Ultraconserved Enhancers Results in Viable Mice

(A) Schematic diagrams of each enhancer knockout line generated using CRISPR/Cas9 editing in fertilized mouse eggs. Ultraconserved forebrain enhancers are shown as blue ovals, with red crosses indicating enhancer deletion alleles. Schematic locus representation is not to scale.

(B) In all cases, loss of individual or pairs of ultraconserved enhancers near *Arx* resulted in viable heterozygous female and hemizygous null male mice (Figure S2) that did not show any obvious embryonic lethality or loss of fertility (Table S4). n.d., not determined; n.s., not significant.

See also Figure S2 and Tables S3 and S4.

pancreatic anomalies (Collombat et al., 2003; Kitamura et al., 2002). In contrast, males lacking any of the single or pairs of ultraconserved *Arx* forebrain enhancers are viable, and none displayed increased lethality *in utero* or perinatally (Figure 3B; Table S4). Furthermore, hemizygous null males from all enhancer deletion lines were capable of siring offspring, ruling out severe infertility or testicular defects (Figure 3B; Table S4). Similarly, heterozygous null females were viable and fertile (Figure 3B; Table S4), and viable homozygous null females were obtained in all cases tested (Figure 3B). All told, individual loss of any of four ultraconserved forebrain enhancers near *Arx* resulted in mice that are both viable and fertile.

Remarkably, mice missing pairs of potentially redundant ultraconserved enhancers are similarly viable and fertile and have no obvious abnormalities (Figure 3B). These results demonstrate that even deletions of the longest ultraconserved sites in the genome do not have broadly catastrophic consequences to an individual organism's viability or fertility, further refuting the assumption that extreme evolutionary sequence constraint translates to indispensable function. These results are additionally inconsistent with the hypothesis that functional redundancy between ultraconserved sites explains the absence of obviously deleterious phenotypes.

Pairwise Loss of Ultraconserved Enhancers Results in Decreased *Arx* RNA

We next examined whether the expression of *Arx* in the developing forebrain is altered upon loss of individual or pairs of ultraconserved enhancers. RNA-seq on whole forebrain from male E11.5 embryos hemizygous null for single or pairs of enhancers showed that both double enhancer deletions result in reduced *Arx* expression ($p \leq 0.002$ by edgeR; see STAR Methods; Figures 4A and 4B; Table S5). No other gene within 10 Mb of the enhancers had significantly reduced expression, indicating that these ultraconserved enhancers act specifically on *Arx*. In contrast to the double knockouts, none of the single enhancer deletions profiled led to substantial downregulation of *Arx,* as measured by RNA-seq (Figure S3).

To further explore how the enhancer deletions affect *Arx* expression in specific subregions of the developing forebrain, and to identify changes that may not be captured by whole tissue mRNA sequencing, we performed *Arx* RNA *in situ* hybridization on embryonic forebrain tissue sections (Figures 4C, 4D, and S4). In all cases where loss of *Arx* expression was observed by RNA-seq, this deficit was in the region of the brain where the enhancers are active. For example, the combined loss of both enhancers active in the ventral telencephalon (hs119/hs121) results in reduced *Arx* expression in the ventral telencephalon. *In situ* hybridization also revealed a reduction of *Arx* expression in the dorsal forebrain of hs122 null embryos that was not detected by RNA-seq (Figures 4D and S4). Together, these results confirm that the four ultraconserved enhancers regulate the brain region-specific expression of *Arx*.

Ultraconserved Enhancer Deletions Cause Growth and Brain Defects

To further explore the phenotypic consequences of the loss of ultraconserved enhancers near *Arx*, we performed a detailed characterization of growth and brain morphology for mice missing single or pairwise enhancer combinations. First, we used postnatal weight gain as a broad proxy for general organismal fitness (Crawley, 2007). While the majority of enhancer deletions resulted in no significant changes in growth, the loss of the hs119 ventral forebrain enhancer resulted in a 5%–10%

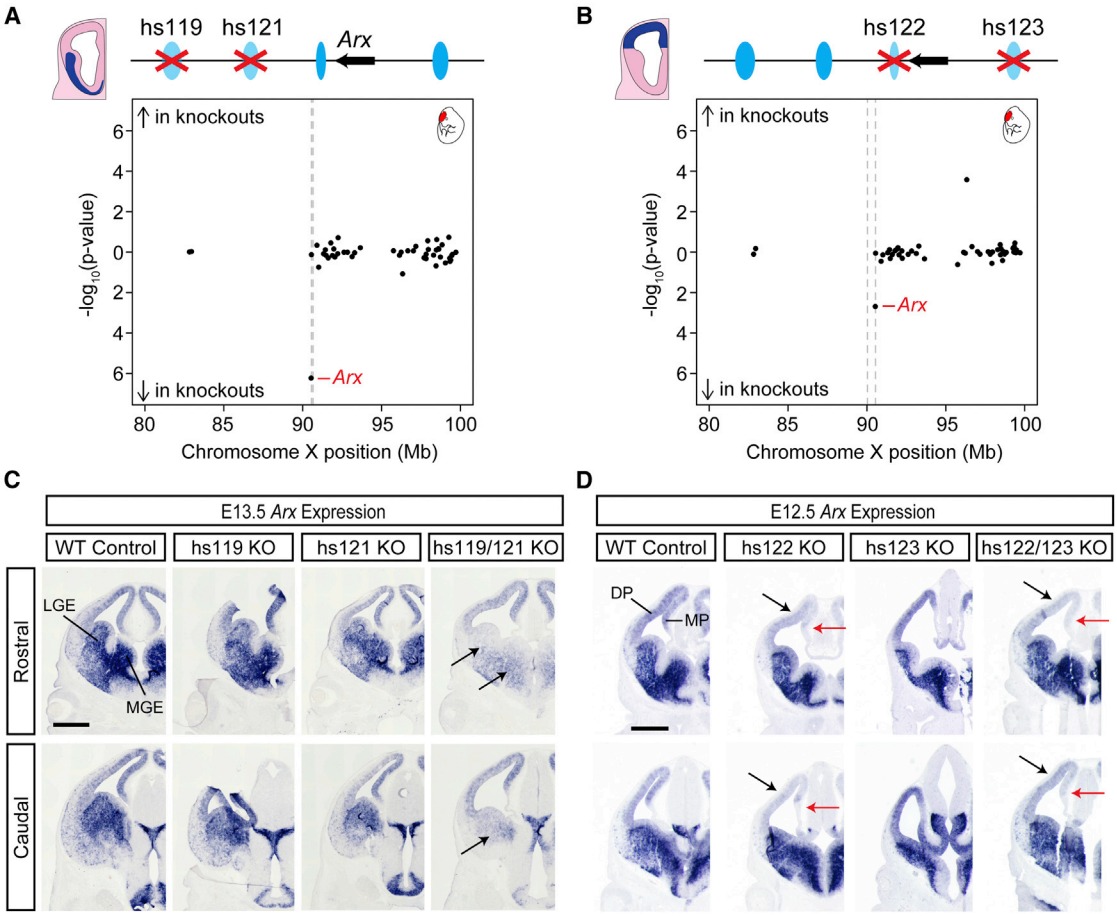

Figure 4. *Arx* Expression Is Diminished in Enhancer Deletion Mice

(A and B) RNA-seq results for double knockouts of hs119/hs121 (A) and hs122/hs123 (B), showing all genes within a 20 Mb window around *Arx*. Whole forebrain from E11.5 embryos was profiled for each pair of deletions (n = 2 wild-type, n = 2 hemizygous null males for each panel). Each point represents an individual gene, with its position on the X chromosome (x axis) and significance of deviation from wild-type (y axis) indicated. Genes with decreased expression in knockout embryos are plotted with $-\log_{10}(p)$ scores below 0. Dashed gray lines mark the positions of the enhancers.

(C) *Arx* expression (blue staining) profiled by *in situ* hybridization in coronal sections of E13.5 forebrain from embryos missing the enhancers active in the ventral forebrain. Embryos missing both enhancers in combination (hs119/hs121 KO) have substantial deficits of *Arx* in the ventral forebrain (black arrows).

(D) *Arx* expression in E12.5 forebrain from embryos missing enhancers active in the dorsal forebrain. Embryos missing both enhancers in combination have decreased *Arx* expression in the dorsal pallium (black arrows) and in the medial pallium (red arrows), with hs122 null embryos having similar changes. Scale bars, 500 μm. LGE, lateral ganglionic eminence; MGE, medial ganglionic eminence; DP, dorsal pallium; MP, medial pallium.

See also Figures S3 and S4 and Table S5.

reduction in body mass (postnatal weeks 6–16, Figures 5A and S5, $p < 0.05$; two-tailed t test). This phenotype was exacerbated by combined loss of both ventral forebrain enhancers (hs119/hs121), which resulted in an ~15% reduction in body weight throughout the entire developmental window examined (Figure 5A, $p < 0.05$ at 17 of 18 postnatal time points measured; two-tailed t test).

Guided by the severe forebrain phenotypes observed in mice hemizygous null for the *Arx* gene (Kitamura et al., 2002), we next screened all lines for neuroanatomical changes, beginning with the ventral enhancer deletions (hs119, hs121, hs119/hs121). Deletion of the *Arx* gene results in defects in the ventral telencephalon, in particular a substantial decrease in striatal cholinergic neurons (Colombo et al., 2007; Marsh et al., 2016). While postnatal (P30–P63) mice lacking the ventral forebrain enhancers showed no obvious change in the overall size or structure of the striatum (Figure 5B), immunohistochemical analysis of choline acetyltransferase (ChAT)-expressing neurons revealed a 62% reduction in the density of cholinergic neurons in the striatum for males missing hs121 (Figures 5B and 5C; Table S6, $p < 0.001$; ANOVA). Males hemizygous null for hs119 and hs121 combined had a near-complete (97%) loss of cholinergic neurons in the striatum (Figures 5B and 5C and Table S6, $p < 0.001$; ANOVA). We also examined the postnatal densities of several neocortical GABAergic interneuron populations that originate in the ventral telencephalon during embryogenesis, some of which are known to be altered in *Arx* gene knockout mice

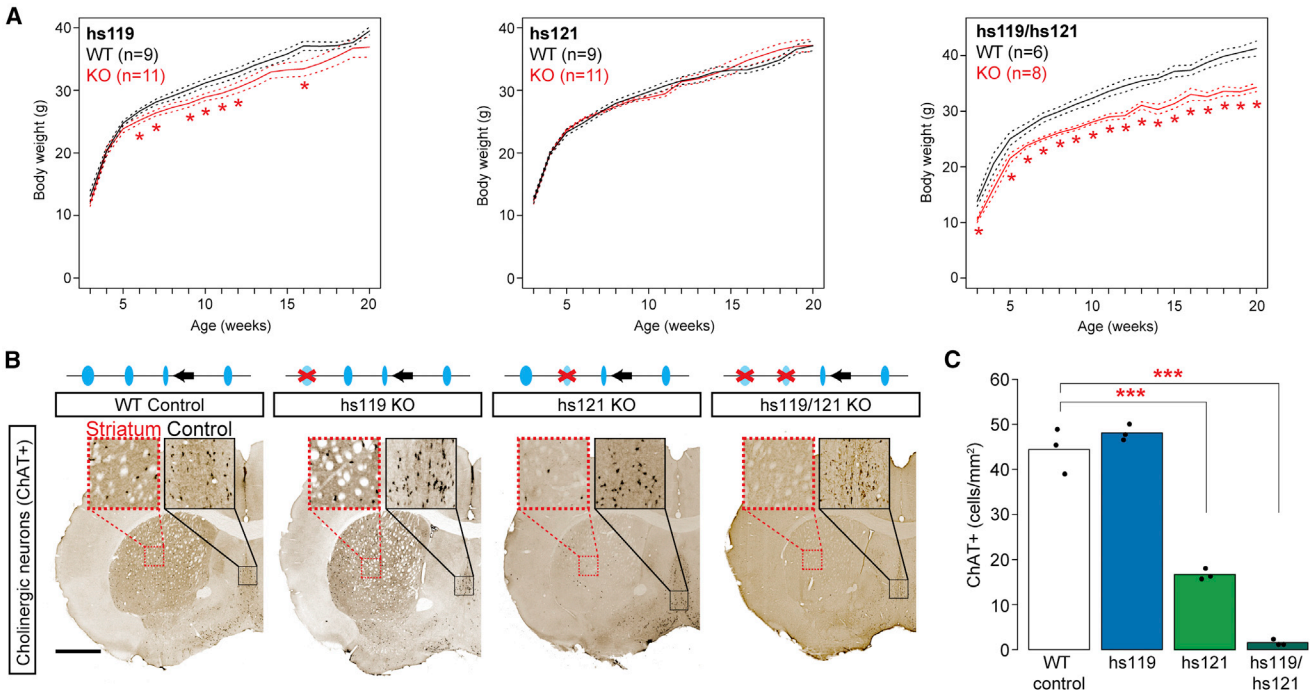

Figure 5. Loss of Ultraconserved Ventral Forebrain Enhancers Results in Growth and Brain Abnormalities

(A) Growth curves for males wild-type (WT, black) or hemizygous null (KO, red) for the ventral forebrain enhancers. Solid lines show mean weight, with dashed lines indicating SEM. Sample sizes are shown on each plot. *$p < 0.05$; two-tailed t test.

(B) Representative coronal cross-sections of postnatal mouse brains stained for choline acetyltransferase (ChAT, black dots) from a wild-type control and males hemizygous null (KO) for the enhancers active in the ventral forebrain. The loss of hs121 alone or hs119/hs121 combined results in decreased density of cholinergic neurons in the striatum (red box insets), whereas ChAT$^+$ populations in other structures are unaffected (black box insets). Scale bar, 1 mm.

(C) Quantification of striatal cholinergic neuron density for ventral enhancer knockouts. Bars indicate group means, while individual points represent biological replicates. ***$p < 0.001$; ANOVA.

See also Figures S5 and S6 and Table S6.

(Colombo et al., 2007; Kitamura et al., 2002). Loss of hs121 alone, or in combination with hs119 (hs119/hs121 KO), resulted in a 21%–24% decrease in the density of parvalbumin (PV)-expressing neocortical interneurons and a moderate (37%–52%) increase in vasointestinal peptide (VIP) interneurons (Figure S6; Table S6, $p < 0.05$; ANOVA). In summary, the individual loss of one ultraconserved ventral telencephalon enhancer (hs121) alone causes substantial alterations in neuron populations in the postnatal mouse brain, and this phenotype further increases in severity when both ventral forebrain enhancers of *Arx* are lost. These results demonstrate a role for both ventral forebrain *Arx* enhancers in the development of specific classes of neurons.

Finally, we assessed neuronal phenotypes resulting from the loss of ultraconserved *Arx* enhancers that are active in the dorsal telencephalon. Brain sections from postnatal hemizygous null males and matched littermate controls (13 to 28 weeks of age) revealed obvious abnormalities to the hippocampus caused by the loss of one of the dorsal enhancers (hs122), consistent with the dysgenesis of the hippocampus observed in *Arx* gene knockouts (Colasante et al., 2015; Kitamura et al., 2002). Specifically, loss of hs122 led to a 26% reduction in the length of the dentate gyrus and a 36% reduction in the area of its granule cell layer ($p < 0.05$; two-tailed t test), in the absence of substantial changes in the length of other hippocampal structures examined (Figures 6A, 6B, and S7; Table S6). Additionally, the dentate gyrus had a severely disorganized appearance in hs122 null mice (Figures 6A, S7A, and S7B). Loss of hs123 alone did not result in any obvious deficits in the hippocampus, and combined loss of hs122 and hs123 resulted in a phenotype similar to hs122 alone (Figures 6A, 6B, and S7; Table S6). Thus, in combination with the ventrally active enhancers, our results reveal a role for three out of four ultraconserved *Arx* enhancers in the development of the brain.

DISCUSSION

Ultraconserved sites have fascinated biologists since their identification, and their perfect extended sequence conservation led to the widespread assumption that these sequences are generally required for organismal viability. However, this is clearly contradicted by deletion studies of individual non-exonic ultraconserved sites, which have uniformly resulted in viable and fertile mice (this study; Ahituv et al., 2007; Nolte et al., 2014). In this study, we sought to explain the puzzling observation that loss of sequences with extreme conservation results in no obvious detrimental effects *in vivo*. By focusing on the numerous and unusually long ultraconserved elements near the essential

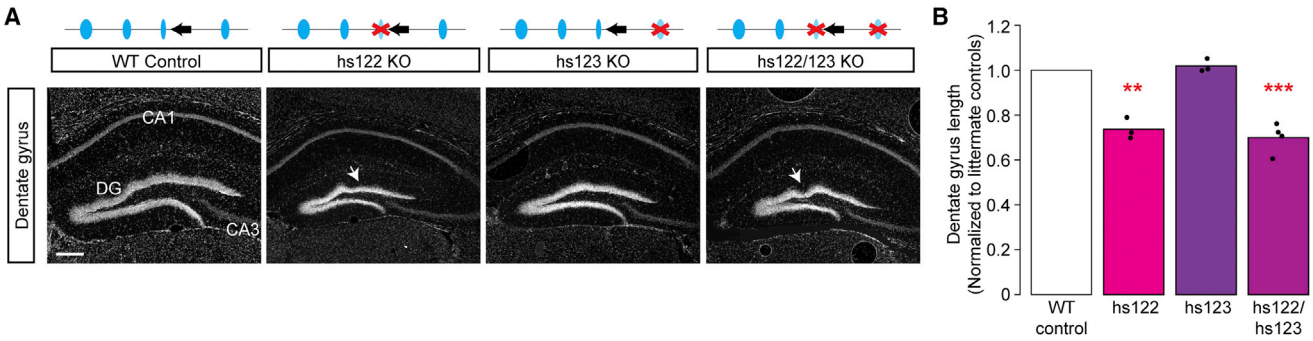

Figure 6. Loss of Ultraconserved Dorsal Forebrain Enhancers Results in Abnormal Brain Development

(A) Representative rostral coronal cross-sections of postnatal hippocampus from a wild-type control, along with males hemizygous null for the enhancers active in the dorsal forebrain. Individual loss of hs122 or combined loss of hs122/hs123 results in a smaller dentate gyrus (DG) with disorganized appearance (white arrowheads). CA1/3: hippocampal *Cornu Ammonis* 1 and 3. Scale bar, 250 μm.

(B) Dentate gyrus length for dorsal forebrain enhancer knockouts normalized to wild-type littermate controls. Bars indicate group means, with individual points showing biological replicates. **p < 0.01; ***p < 0.001; two-tailed t test.

See also Figure S7 and Table S6.

Arx gene, we were able to assess whether functional redundancy between ultraconserved enhancers or the presence of nonlethal, but nonetheless detrimental, phenotypes is most likely to explain this surprising observation. We deleted pairs of potentially redundant enhancers with similar activity profiles, removing up to 2,086 bp (hs119 + hs121) of perfectly human-rodent conserved sequence. Surprisingly, even this combinatorial removal of extremely long ultraconserved enhancers yielded viable and fertile mice, undermining the hypothesis that functional redundancy is the primary explanation for the lack of obvious viability deficits. These results further underscore that perfect conservation is not analogous to essentiality.

In the absence of the conclusive identification of phenotypes explained by the loss of tissue-specific enhancers for previous ultraconserved site knockouts, a variety of alternative hypotheses to explain the extreme conservation at these sites were proposed, some of which were not based on the conventional model of negative selection (Chiang et al., 2008; Harmston et al., 2013). In this study, we identified important biological functions for the majority of individual ultraconserved sites examined. Namely, individual loss of three of the four ultraconserved enhancers examined resulted in a deficit of growth or neurodevelopment (Figure 7). We posit that negative selection against these detrimental phenotypes is likely at least partly responsible for the conservation observed. For this study, we focused on ultraconserved enhancers that are located on the X chromosome and exclusively examined hemizygous male mice. This raises the question whether the heterozygous loss of ultraconserved enhancers, either for X chromosome loci in females or for autosomal loci generally, will also broadly result in identifiable

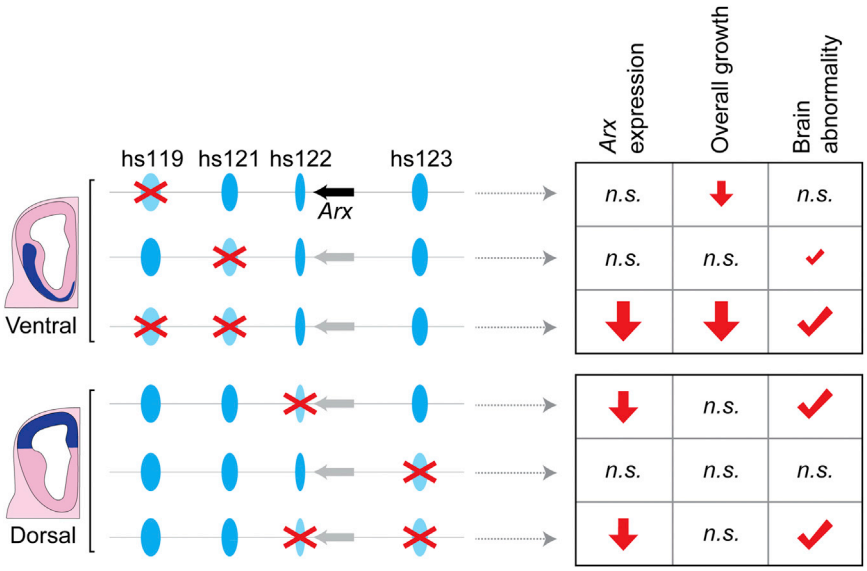

Figure 7. Summary of Phenotypes Resulting from Loss of Ultraconserved *Arx* Enhancers

n.s., no significant changes observed.

phenotypes. Based on previous mouse knockouts of less well conserved autosomal enhancers, we speculate that heterozygous loss of some ultraconserved enhancers will be sufficient to cause similar, albeit less severe, developmental phenotypes and deficits in gene expression (Dickel et al., 2016; Johnson et al., 2012). Collectively, these results support that loss of ultraconserved elements leads to fitness defects that are generally subtle in a laboratory setting but likely selected against over evolutionary time.

STAR★METHODS

Detailed methods are provided in the online version of this paper and include the following:

- KEY RESOURCES TABLE
- CONTACT FOR REAGENT AND RESOURCE SHARING
- EXPERIMENTAL MODEL AND SUBJECT DETAILS
- METHOD DETAILS
  - Ultraconserved Sequence Annotations
  - Generating Transgenic Embryos
  - Single-Cell RNA-Seq
  - Generation of Enhancer Knockout Mice
  - RNA-Seq for Enhancer Knockouts
  - *In situ* Hybridization
  - Body Weight Measurements
  - Sample Selection for Neurological Phenotyping
  - Brain Sectioning and Immunohistochemistry
  - Image Acquisition and Analysis
  - Cell Counting
  - Hippocampal Measurements
- QUANTIFICATION AND STATISTICAL ANALYSIS
- DATA AND SOFTWARE AVAILABILITY

SUPPLEMENTAL INFORMATION

Supplemental Information includes seven figures and seven tables and can be found with this article online at https://doi.org/10.1016/j.cell.2017.12.017.

ACKNOWLEDGMENTS

We would like to thank qb3 MacroLab for plasmid pML6B and J. Doudna (University of California Berkeley) for plasmid pMJ920 and for advice on Cas9/CRISPR-mediated genome editing. This work used the Vincent J. Coates Genomics Sequencing Laboratory at UC Berkeley, which is supported by NIH grants S10RR029668 and S10RR027303. Research was conducted at the E.O. Lawrence Berkeley National Laboratory and performed under U.S. Department of Energy contract DE-AC02-05CH11231, University of California. This work was supported by NIH grants to L.A.P. and A.V. (R01HG003988, R24HL123879, and UM1HL098166) and to J.L.R.R. (NINDS R01NS34661 and NIMH R37MH049428). The single-cell RNA sequencing work was supported by the Laboratory Directed Research and Development Program of Lawrence Berkeley National Laboratory (to D.E.D.). A.R.Y. was supported by a grant from Fondation Fyssen. M.O. was supported by a Swiss National Science Foundation (SNSF) fellowship.

AUTHOR CONTRIBUTIONS

D.E.D., A.R.Y., R.P., Y.Z., B.J.M., Y.S.K., I.P.-F., C.S.P., E.A.L., A.N.H., Q.T.P., T.H.G., M.K., M.O., J.A.A., and V.A. performed experiments, including making and/or characterizing all transgenic and knockout mouse lines. D.E.D., I.B., and Y.F.-Y. analyzed RNA-seq data. D.E.D., A.R.Y., R.P., J.L.R.R., L.A.P., and A.V. planned the study and wrote the manuscript with input from the remaining authors.

DECLARATION OF INTERESTS

J.L.R.R. is cofounder, stockholder, and currently on the scientific board of Neurona, a company studying the potential therapeutic use of interneuron transplantation.

Received: August 11, 2017
Revised: October 27, 2017
Accepted: December 11, 2017
Published: January 18, 2018

REFERENCES

Adams, J.C. (1981). Heavy metal intensification of DAB-based HRP reaction product. J. Histochem. Cytochem. *29*, 775.

Ahituv, N., Zhu, Y., Visel, A., Holt, A., Afzal, V., Pennacchio, L.A., and Rubin, E.M. (2007). Deletion of ultraconserved elements yields viable mice. PLoS Biol. *5*, e234.

Anders, S., Pyl, P.T., and Huber, W. (2015). HTSeq–a Python framework to work with high-throughput sequencing data. Bioinformatics *31*, 166–169.

Bejerano, G., Pheasant, M., Makunin, I., Stephen, S., Kent, W.J., Mattick, J.S., and Haussler, D. (2004). Ultraconserved elements in the human genome. Science *304*, 1321–1325.

Benjamini, Y., and Hochberg, Y. (1995). Controlling the false discovery rate: a practical and powerful approach to multiple testing. J. R. Stat. Soc. Series B Stat. Methodol. *57*, 289–300.

Chen, Y.-J.J., Friedman, B.A., Ha, C., Durinck, S., Liu, J., Rubenstein, J.L., Seshagiri, S., and Modrusan, Z. (2017). Single-cell RNA sequencing identifies distinct mouse medial ganglionic eminence cell types. Sci. Rep. *7*, 45656.

Chiang, C.W.K., Derti, A., Schwartz, D., Chou, M.F., Hirschhorn, J.N., and Wu, C.-T. (2008). Ultraconserved elements: analyses of dosage sensitivity, motifs and boundaries. Genetics *180*, 2277–2293.

Colasante, G., Collombat, P., Raimondi, V., Bonanomi, D., Ferrai, C., Maira, M., Yoshikawa, K., Mansouri, A., Valtorta, F., Rubenstein, J.L.R., and Broccoli, V. (2008). Arx is a direct target of Dlx2 and thereby contributes to the tangential migration of GABAergic interneurons. J. Neurosci. *28*, 10674–10686.

Colasante, G., Simonet, J.C., Calogero, R., Crispi, S., Sessa, A., Cho, G., Golden, J.A., and Broccoli, V. (2015). ARX regulates cortical intermediate progenitor cell expansion and upper layer neuron formation through repression of Cdkn1c. Cereb. Cortex *25*, 322–335.

Collombat, P., Mansouri, A., Hecksher-Sorensen, J., Serup, P., Krull, J., Gradwohl, G., and Gruss, P. (2003). Opposing actions of Arx and Pax4 in endocrine pancreas development. Genes Dev. *17*, 2591–2603.

Colombo, E., Collombat, P., Colasante, G., Bianchi, M., Long, J., Mansouri, A., Rubenstein, J.L.R., and Broccoli, V. (2007). Inactivation of Arx, the murine ortholog of the X-linked lissencephaly with ambiguous genitalia gene, leads to severe disorganization of the ventral telencephalon with impaired neuronal migration and differentiation. J. Neurosci. *27*, 4786–4798.

Crawley, J.N. (2007). What's Wrong With My Mouse?: Behavioral Phenotyping of Transgenic and Knockout Mice (Wiley).

del Río, J.A., de Lecea, L., Ferrer, I., and Soriano, E. (1994). The development of parvalbumin-immunoreactivity in the neocortex of the mouse. Brain Res. Dev. Brain Res. *81*, 247–259.

Dickel, D.E., Barozzi, I., Zhu, Y., Fukuda-Yuzawa, Y., Osterwalder, M., Mannion, B.J., May, D., Spurrell, C.H., Plajzer-Frick, I., Pickle, C.S., et al. (2016). Genome-wide compendium and functional assessment of in vivo heart enhancers. Nat. Commun. *7*, 12923.

Dobin, A., Davis, C.A., Schlesinger, F., Drenkow, J., Zaleski, C., Jha, S., Batut, P., Chaisson, M., and Gingeras, T.R. (2013). STAR: ultrafast universal RNA-seq aligner. Bioinformatics *29*, 15–21.

Ester, M., Kriegel, H.P., Sander, J., and Xu, X. (1996). A density-based algorithm for discovering clusters in large spatial databases with noise. KDD *96*, 226–231.

Finak, G., McDavid, A., Yajima, M., Deng, J., Gersuk, V., Shalek, A.K., Slichter, C.K., Miller, H.W., McElrath, M.J., Prlic, M., et al. (2015). MAST: a flexible statistical framework for assessing transcriptional changes and characterizing heterogeneity in single-cell RNA sequencing data. Genome Biol. *16*, 278.

Gécz, J., Cloosterman, D., and Partington, M. (2006). ARX: a gene for all seasons. Curr. Opin. Genet. Dev. *16*, 308–316.

Gould, E., Woolf, N.J., and Butcher, L.L. (1991). Postnatal development of cholinergic neurons in the rat: I. Forebrain. Brain Res. Bull. *27*, 767–789.

Harmston, N., Baresic, A., and Lenhard, B. (2013). The mystery of extreme non-coding conservation. Philos. Trans. R. Soc. Lond. B Biol. Sci. *368*, 20130021.

Harrow, J., Frankish, A., Gonzalez, J.M., Tapanari, E., Diekhans, M., Kokocinski, F., Aken, B.L., Barrell, D., Zadissa, A., Searle, S., et al. (2012). GENCODE: the reference human genome annotation for The ENCODE Project. Genome Res. *22*, 1760–1774.

Hsu, F., Kent, W.J., Clawson, H., Kuhn, R.M., Diekhans, M., and Haussler, D. (2006). The UCSC known genes. Bioinformatics *22*, 1036–1046.

Johnson, K.D., Hsu, A.P., Ryu, M.-J., Wang, J., Gao, X., Boyer, M.E., Liu, Y., Lee, Y., Calvo, K.R., Keles, S., et al. (2012). Cis-element mutated in GATA2-dependent immunodeficiency governs hematopoiesis and vascular integrity. J. Clin. Invest. *122*, 3692–3704.

Kiselev, V.Y., Kirschner, K., Schaub, M.T., Andrews, T., Yiu, A., Chandra, T., Natarajan, K.N., Reik, W., Barahona, M., Green, A.R., and Hemberg, M. (2017). SC3: consensus clustering of single-cell RNA-seq data. Nat. Methods *14*, 483–486.

Kitamura, K., Yanazawa, M., Sugiyama, N., Miura, H., Iizuka-Kogo, A., Kusaka, M., Omichi, K., Suzuki, R., Kato-Fukui, Y., Kamiirisa, K., et al. (2002). Mutation of ARX causes abnormal development of forebrain and testes in mice and X-linked lissencephaly with abnormal genitalia in humans. Nat. Genet. *32*, 359–369.

Kothary, R., Clapoff, S., Darling, S., Perry, M.D., Moran, L.A., and Rossant, J. (1989). Inducible expression of an hsp68-lacZ hybrid gene in transgenic mice. Development *105*, 707–714.

Kvon, E.Z., Kamneva, O.K., Melo, U.S., Barozzi, I., Osterwalder, M., Mannion, B.J., Tissières, V., Pickle, C.S., Plajzer-Frick, I., Lee, E.A., et al. (2016). Progressive loss of function in a limb enhancer during snake evolution. Cell *167*, 633–642.

Macosko, E.Z., Basu, A., Satija, R., Nemesh, J., Shekhar, K., Goldman, M., Tirosh, I., Bialas, A.R., Kamitaki, N., Martersteck, E.M., et al. (2015). Highly parallel genome-wide expression profiling of individual cells using nanoliter droplets. Cell *161*, 1202–1214.

Mali, P., Yang, L., Esvelt, K.M., Aach, J., Guell, M., DiCarlo, J.E., Norville, J.E., and Church, G.M. (2013). RNA-guided human genome engineering via Cas9. Science *339*, 823–826.

Marsh, E.D., Nasrallah, M.P., Walsh, C., Murray, K.A., Nicole Sunnen, C., McCoy, A., and Golden, J.A. (2016). Developmental interneuron subtype deficits after targeted loss of Arx. BMC Neurosci. *17*, 35.

Martin, M. (2011). Cutadapt removes adapter sequences from high-throughput sequencing reads. EMBnet.Journal *17*, 10–12.

McLean, C., and Bejerano, G. (2008). Dispensability of mammalian DNA. Genome Res. *18*, 1743–1751.

Motenko, H., Neuhauser, S.B., O'Keefe, M., and Richardson, J.E. (2015). MouseMine: a new data warehouse for MGI. Mamm. Genome *26*, 325–330.

Nolte, M.J., Wang, Y., Deng, J.M., Swinton, P.G., Wei, C., Guindani, M., Schwartz, R.J., and Behringer, R.R. (2014). Functional analysis of limb transcriptional enhancers in the mouse. Evol. Dev. *16*, 207–223.

Pennacchio, L.A., Ahituv, N., Moses, A.M., Prabhakar, S., Nobrega, M.A., Shoukry, M., Minovitsky, S., Dubchak, I., Holt, A., Lewis, K.D., et al. (2006). In vivo enhancer analysis of human conserved non-coding sequences. Nature *444*, 499–502.

Pruitt, K.D., Tatusova, T., and Maglott, D.R. (2005). NCBI Reference Sequence (RefSeq): a curated non-redundant sequence database of genomes, transcripts and proteins. Nucleic Acids Res. *33*, D501–D504.

Robinson, M.D., McCarthy, D.J., and Smyth, G.K. (2010). edgeR: a Bioconductor package for differential expression analysis of digital gene expression data. Bioinformatics *26*, 139–140.

Rosenbloom, K.R., Armstrong, J., Barber, G.P., Casper, J., Clawson, H., Diekhans, M., Dreszer, T.R., Fujita, P.A., Guruvadoo, L., Haeussler, M., et al. (2015). The UCSC Genome Browser database: 2015 update. Nucleic Acids Res. *43*, D670–D681.

Sandelin, A., Bailey, P., Bruce, S., Engström, P.G., Klos, J.M., Wasserman, W.W., Ericson, J., and Lenhard, B. (2004). Arrays of ultraconserved non-coding regions span the loci of key developmental genes in vertebrate genomes. BMC Genomics *5*, 99.

Schneider, C.A., Rasband, W.S., and Eliceiri, K.W. (2012). NIH Image to ImageJ: 25 years of image analysis. Nat. Methods *9*, 671–675.

Sing, T., Sander, O., Beerenwinkel, N., and Lengauer, T. (2005). ROCR: visualizing classifier performance in R. Bioinformatics *21*, 3940–3941.

Stanco, A., Pla, R., Vogt, D., Chen, Y., Mandal, S., Walker, J., Hunt, R.F., Lindtner, S., Erdman, C.A., Pieper, A.A., et al. (2014). NPAS1 represses the generation of specific subtypes of cortical interneurons. Neuron *84*, 940–953.

Taniguchi, H., He, M., Wu, P., Kim, S., Paik, R., Sugino, K., Kvitsiani, D., Fu, Y., Lu, J., Lin, Y., et al. (2011). A resource of Cre driver lines for genetic targeting of GABAergic neurons in cerebral cortex. Neuron *71*, 995–1013.

Trapnell, C., Pachter, L., and Salzberg, S.L. (2009). TopHat: discovering splice junctions with RNA-Seq. Bioinformatics *25*, 1105–1111.

Trapnell, C., Williams, B.A., Pertea, G., Mortazavi, A., Kwan, G., van Baren, M.J., Salzberg, S.L., Wold, B.J., and Pachter, L. (2010). Transcript assembly and quantification by RNA-Seq reveals unannotated transcripts and isoform switching during cell differentiation. Nat. Biotechnol. *28*, 511–515.

Visel, A., Prabhakar, S., Akiyama, J.A., Shoukry, M., Lewis, K.D., Holt, A., Plajzer-Frick, I., Afzal, V., Rubin, E.M., and Pennacchio, L.A. (2008). Ultraconservation identifies a small subset of extremely constrained developmental enhancers. Nat. Genet. *40*, 158–160.

Visel, A., Taher, L., Girgis, H., May, D., Golonzhka, O., Hoch, R.V., McKinsey, G.L., Pattabiraman, K., Silberberg, S.N., Blow, M.J., et al. (2013). A high-resolution enhancer atlas of the developing telencephalon. Cell *152*, 895–908.

Wang, H., Yang, H., Shivalila, C.S., Dawlaty, M.M., Cheng, A.W., Zhang, F., and Jaenisch, R. (2013). One-step generation of mice carrying mutations in multiple genes by CRISPR/Cas-mediated genome engineering. Cell *153*, 910–918.

Wang, B., Zhu, J., Pierson, E., Ramazzotti, D., and Batzoglou, S. (2017). Visualization and analysis of single-cell RNA-seq data by kernel-based similarity learning. Nat. Methods *14*, 414–416.

Yang, H., Wang, H., Shivalila, C.S., Cheng, A.W., Shi, L., and Jaenisch, R. (2013). One-step generation of mice carrying reporter and conditional alleles by CRISPR/Cas-mediated genome engineering. Cell *154*, 1370–1379.

STAR★METHODS

KEY RESOURCES TABLE

REAGENT or RESOURCE	SOURCE	IDENTIFIER
Antibodies		
rabbit anti-parvalbumin	Swant Swiss Abs	Cat# PV 28
rat anti-somatostatin (clone YC7)	Millipore	Cat# MAB354
goat anti-somatostatin (D-20)	Santa Cruz	Cat# sc-7819
rabbit anti-Vasointestinal peptide	Immunostar	Cat# 20077; RRID: AB_572270
goat anti-Choline Acetyltransferase (ChAT)	Millipore	Cat# AB144P
mouse Anti-Calretinin, (clone 6B8.2)	Millipore	Cat# MAB1568
Anti-Digoxigenin-AP, Fab fragments	Roche	Cat# 11093274910
Chemicals, Peptides, and Recombinant Proteins		
DIG RNA labeling mix	Roche	Cat# 11277073910
T3 polymerase	Roche	Cat# RPOLT3-RO
DNaseI	Roche	Cat# 4716728001
Sheep serum	Sigma	Cat# S2263
Blocking reagent	Roche	Cat# 11096176001
BM Purple	Roche	Cat# 11442074001
Accumax Cell Dissociation Solution	Innovative Cell Technologies	Cat# AM105
Maxima H Minus Reverse Transcriptase	Thermo Fisher Scientific	Cat# EP0753
Perfluorooctanol	Sigma	Cat# 370533-25G
Exonuclease I	New England Biolabs	Cat# M0293L
Critical Commercial Assays		
RNA Clean & Concentrator	Zymo Research	Cat# R1015
mMESSAGE mMACHINE T7 kit	Thermo Fisher Scientific	Cat# AM1344
MEGAshortscript T7 kit	Thermo Fisher Scientific	Cat# AM1354
MEGAclear kit	Thermo Fisher Scientific	Cat# AM1908
Barcoded dT Beads for Drop-Seq	Macosko et al., 2015 ChemGenes	Lot# 011416B
TruSeq Stranded mRNA Sample Prep Kit	Illumina	Cat# RS-122-2101
RNAqueous Total RNA Isolation Kit	Thermo Fisher Scientific	Cat# AM1912
Drop-seq Microfluidic Device	Macosko et al., 2015 Nanoshift	N/A
KAPA HiFi HotStart ReadyMix	Kapa Biosystems	Cat# KK2602
Nextera XT DNA Library Preparation Kit	Illumina	Cat# FC-131-1096
TURBO DNA-free Kit	Thermo Fisher Scientific	Cat# AM1907
Deposited Data		
RNA-seq data, including Drop-seq for enhancer transgenics, and bulk tissue RNA-seq for enhancer knockouts	This paper	GEO: GSE100394
Experimental Models: Organisms/Strains		
Mouse: FVB	Charles River	https://www.criver.com/
Mouse: FVB/*Arx*-Δhs119	This paper	N/A
Mouse: FVB/*Arx*-Δhs121	This paper	N/A
Mouse: FVB/*Arx*-Δhs122	This paper	N/A
Mouse: FVB/*Arx*-Δhs123	This paper	N/A
Mouse: FVB/*Arx*-Δhs119Δhs121	This paper	N/A
Mouse: FVB/*Arx*-Δhs122Δhs123	This paper	N/A

(*Continued on next page*)

Continued

REAGENT or RESOURCE	SOURCE	IDENTIFIER
Oligonucleotides		
A full list of primers and oligos is provided in Table S7	IDT	N/A
Recombinant DNA		
Hsp68-mCherry vector	This paper	N/A; available from the authors
Hsp68-GFP vector	This paper	N/A; available from the authors
hs119-hsp68-GFP reporter vector	This paper	N/A; available from the authors
hs121-hsp68-mCherry reporter vector	This paper	N/A; available from the authors
hs122-hsp68-GFP reporter vector	This paper	N/A; available from the authors
hs123-hsp68-mCherry reporter vector	This paper	N/A; available from the authors
pDD921 plasmid encoding human optimized Cas9	Kvon et al., 2016	N/A; available from the authors
gRNA cloning vector	Mali et al., 2013	Addgene Plasmid #41824
Software and Algorithms		
Drop-seq published pipeline v. 1.11	Macosko et al., 2015	http://www.mccarrolllab.com/dropseq/
STAR v. 2.4.1d	Dobin et al., 2013	https://github.com/alexdobin/STAR
SIMLR	Wang et al., 2017	http://bioconductor.org/packages/release/bioc/html/SIMLR.html
DBSCAN	Ester et al., 1996	https://cran.r-project.org/web/packages/dbscan/
MAST	Finak et al., 2015	https://github.com/RGLab/MAST
ROCR	Sing et al., 2005	https://cran.r-project.org/web/packages/ROCR/
cutadapt_v1.1	Martin, 2011	https://github.com/marcelm/cutadapt
TopHat v2.0.6	Trapnell et al., 2009	https://github.com/infphilo/tophat
HTSeq	Anders et al., 2015	https://github.com/simon-anders/htseq
edgeR	Robinson et al., 2010	http://bioconductor.org/packages/release/bioc/html/edgeR.html
Cufflinks v2.2.1	Trapnell et al., 2010	https://github.com/cole-trapnell-lab/cufflinks
ImageJ	Schneider et al., 2012	https://imagej.nih.gov/ij/
SPSS Statistics v15	SPSS Inc.	https://www.ibm.com/products/spss-statistics
Other		
Guide RNA cloning protocol	Mali et al., 2013	https://media.addgene.org/cms/files/hCRISPR_gRNA_Synthesis.pdf
List of human-mouse-rat ultraconserved sequences	Bejerano et al., 2004	https://users.soe.ucsc.edu/~jill/ultra.html
Drop-Seq experimental protocol	Macosko et al., 2015	http://mccarrolllab.com/dropseq/

CONTACT FOR REAGENT AND RESOURCE SHARING

Further information and requests for reagents may be directed to, and will be fulfilled by Lead Contact Axel Visel (avisel@lbl.gov).

EXPERIMENTAL MODEL AND SUBJECT DETAILS

All animal work was reviewed and approved by the Lawrence Berkeley National Laboratory Animal Welfare and Research Committee. All mice used in this study were housed at the Animal Care Facility (ACF) of LBNL. Mice were monitored daily for food and water intake, and animals were inspected weekly by the Chair of the Animal Welfare and Research Committee and the head of the animal facility in consultation with the veterinary staff. The LBNL ACF is accredited by the American Association for the Accreditation of Laboratory Animal Care (AAALAC). All transgenic and knockout mouse models generated as part of this work were made in the *Mus musculus* FVB strain.

Transgenic (enhancer-reporter) embryos used for Drop-seq were developmental stage E12.5. These embryos were not assessed for gender, which is not outwardly obvious at E12.5. Therefore, we expect that a roughly equal number of male and female embryos were assessed. Additional information is provided in the METHOD DETAIL section below (see *Generating Transgenic Embryos* and *Single-Cell RNA-Seq*).

Knockout (enhancer deletion) animals phenotyped were the following ages: RNA-seq (E11.5), *in situ* hybridization (E12.5 for dorsal knockouts, E13.5 for ventral knockouts), body weight phenotyping (3-20 weeks postnatal), neurological phenotyping (postnatal ages from P30 to adult, exact ages of animals are given in Table S6). Phenotyping of enhancer deletion mice was restricted to males because the enhancers deleted reside on the X chromosome, which is subject to random inactivation in females. Additional detailed information regarding specific phenotyping analyses, including selection criteria, is provided in the METHOD DETAIL section below (beginning at *Generation of Enhancer Knockout Mice*).

METHOD DETAILS

Ultraconserved Sequence Annotations

The complete list of human-mouse-rat ultraconserved sequences (Bejerano et al., 2004) was downloaded from https://users.soe.ucsc.edu/~jill/ultra.html. Genomic coordinates were converted to the hg19 human genome assembly using liftOver (Rosenbloom et al., 2015). Current functional annotations (exonic versus non-exonic) of all ultraconserved elements were obtained by using the UCSC Genome Browser's Table Browser function (Rosenbloom et al., 2015) to intersect all ultraconserved sites with hg19 gene annotations, including RefSeq (Pruitt et al., 2005), UCSC Genes (Hsu et al., 2006), and GENCODE v24lift37 (Harrow et al., 2012). Intersections were performed on June 26, 2017. Ultraconserved elements were annotated as exonic if they displayed any overlap with an exon of an annotated gene from any of the gene sets considered. Otherwise, ultraconserved elements were annotated as non-exonic.

Generating Transgenic Embryos

Enhancer names (hs numbers) used are the unique identifiers from the VISTA Enhancer Browser (https://enhancer.lbl.gov/). All four enhancers were previously tested in transgenic mouse assays using a minimal promoter and LacZ reporter gene, and the results for whole mount embryos (Pennacchio et al., 2006) and sectioned forebrain tissue (Visel et al., 2013) were reported previously. For Drop-Seq, transgenic enhancer-reporter embryos were generated using the same techniques (Kothary et al., 1989; Pennacchio et al., 2006), with the exception of a fluorescent transgene (mCherry or GFP) in place of LacZ. Briefly, enhancers were PCR amplified (primers in Table S7) and cloned into a fluorescent reporter vector via the Gateway cloning method (Thermo Fisher Scientific). Transgenic mice were generated using *Mus musculus* FVB strain mice, and sample sizes were determined empirically based on our experience performing > 2,000 transgenic enhancer assays and on the tissue volume requirements of the single-cell RNA-Seq method. Mouse embryos were excluded from further analysis if they did not express the fluorescent reporter gene or were not at the correct developmental stage. As no direct comparisons were made between embryos with and without the enhancer-reporter transgene, randomization and experimenter blinding were unnecessary and not performed.

Single-Cell RNA-Seq

F0 (hs119, hs121, hs122) or F1 (hs123) generation embryos aged E12.5 were screened for fluorescent reporter transgene expression using an MZ16 Stereomicroscope (Leica Microsystems) outfitted with a SOLA SM 365 Light Source (Lumencor). Whole forebrain tissue was dissected from all embryos displaying fluorescent reporter activity in a pattern identical to the previously described enhancer activity pattern. For each enhancer, forebrain tissue from at least two independent founders or founder lines was pooled together. Room temperature Accumax Cell Dissociation Solution (Innovative Cell Technologies) was added to the tissue, and this was briefly pipetted to generate single cell suspensions. Cells were then immediately passed through a 40 micron strainer to remove non-dissociated tissue. Samples were kept on ice throughout the collection and preparation process to prevent RNA degradation. For each experiment, human HEK293T/17 cells (ATCC) were spiked in to a final concentration of 2.5% to serve as an internal quality control for doublet frequency. The final cell concentration was then adjusted to 50 cells/μl. Single-cell RNA sequencing was performed using the Drop-Seq method (Macosko et al., 2015) according to protocol version 3.1 from http://mccarrolllab.com/dropseq/. Briefly, cells and ChemGenes Beads (Lot 011416B) were captured in aqueous droplets containing lysis buffer using a microfluidic device (Nanoshift). Droplets were recovered and broken with the addition of 6X SSC and perfluorooctanol (Sigma) followed by mixing and centrifugation. Beads released from the droplets were recovered, washed, and suspended in reverse transcriptase buffer. Captured mRNAs were reverse transcribed using Maxima H- Reverse Transcriptase (Thermo Fisher Scientific). Beads were then washed, and excess bead primers were removed with Exonuclease I (NEB). Beads were again washed and counted. Template switching PCR was performed using Kapa HiFi Hotstart Readymix (Kapa Biosystems). cDNAs were captured and purified using AMPure XP beads (Beckman Coulter), and library quality was assessed using a BioAnalyzer High Sensitivity Assay (Agilent). Sequencing libraries were generated using the Nextera XT kit (Illumina), purified with AMPure beads, and sequenced paired-end on an Illumina HiSeq2500.

Raw data analysis and digital expression quantification was carried out using the Drop-Seq published pipeline version 1.11 (Macosko et al., 2015). *DetectBeadSynthesisErrors* and *DigitalExpression* were run setting *NUM_CORE_BARCODES* to 10,000.

The alignment was performed using STAR version 2.4.1d (Dobin et al., 2013). Custom genomes and transcriptomes were generated using iGenome annotations for mm10 and hg19, along with the sequences of the transgenes, mCherry and GFP (SUN1-sfGFP). All the downstream analyses were performed using the statistical computing environment R v.3.3.1 (www.r-project.org). First, for each one of the five libraries, the expression counts for each transcript was retrieved for the top 10,000 STAMPs. By means of the human cells spiked-in, the purity was determined using 90% as cutoff (namely, if 90% or more of the transcripts assigned to a STAMP were from human or mouse, that STAMP was assigned to either a human or a mouse cell, otherwise it was considered as a doublet). Next, starting from the 50 STAMPs showing the highest number of detected transcripts, the doublet-rate was estimated (Macosko et al., 2015). The 51st STAMP was then added and the doublet-rate re-calculated, and so forth up to the 10,000th STAMP. A threshold of 10% doublet-rate was finally applied to the resulting curve, which in turn allowed the identification of a set of high-quality STAMPs. A further threshold on the minimum number of detected transcripts was applied, so that STAMPs showing less than 1,000 detected molecules were discarded. Results from the five libraries were then merged together. Digital expression for each STAMP was normalized to Transcripts Per Million (TPM). The expression of the two transgenes (mCherry, GFP) was excluded from any of the following clustering steps. Genes with detectable expression in less than or equal to 10 STAMPs were also discarded. Dimensionality reduction was performed using the *single-cell interpretation via multikernel learning* approach (SIMLR; Wang et al., 2017). The STAMPs were then clustered in the resulting two-dimensional space using density-based clustering (DBSCAN; Ester et al., 1996). The *dbscan* R package was employed, setting *eps* to 3 and *minPts* to 25. MAST (Finak et al., 2015) was then run to detect differentially expressed genes. The Two-sample Likelihood Ratio Test implemented in the *LRT* function of the *MAST* R package allowed the identification of marker genes for each cluster. Briefly, given a cluster, each STAMP was either flagged as belonging or not belonging to it. Those genes identified as upregulated in the cluster at a FDR $\leq$ 0.05 (Benjamini-Hochberg correction; Benjamini and Hochberg, 1995) were classified as markers for the cluster. More stringent sets of marker genes were determined by filtering these lists based on the Area Under the Curve (AUC), which is an estimate of how well a certain gene predicts a cell as belonging to a certain cluster. AUCs were calculated using the *ROCR* R package (Sing et al., 2005). Given a cluster, a list of stringent markers was defined as those genes identified by MAST (see above) also showing an AUC > = 0.6. Enriched pathways and gene ontologies were identified using mouseMine (Motenko et al., 2015). Cell type cluster identities were determined by examining the enriched gene ontology lists and by comparing marker gene sets for each cell type to marker genes used previously for forebrain (such as Chen et al., 2017). The identification of the cell types in which each enhancer is active was robust to the choice of clustering algorithm, as similar analyses using the *k*-means based SC3 method (Kiselev et al., 2017), resulted in identical conclusions.

As a bulk tissue control, whole forebrain from E12.5 littermates not expressing the reporter gene was dissected, pooled, and RNA was extracted using the RNAqueous Total RNA Isolation Kit (Thermo Fisher Scientific). Resulting total RNA was incubated with ChemGenes Beads to specifically capture mRNA. Reverse transcription, library generation, and sequencing for the bulk control were carried out as described for the Drop-Seq libraries (see above). Pseudobulk profiles for each Drop-Seq library were generated by calculating the sum of the single-cell counts for each gene. The resulting profiles were normalized as TPM (transcripts per million sequenced UMIs) and compared to FPKM values from the bulk tissue control. Gene expression correlation values between pseudobulk and bulk are reported in Table S1.

Generation of Enhancer Knockout Mice

Arx enhancer knockout mice were generated using *in vivo* Cas9 editing methods adapted from those previously reported (Wang et al., 2013; Yang et al., 2013) (Figure S2). Briefly, Cas9 was amplified from plasmid pDD921 using primers T7Cas9_F and PolyACas9_R (Kvon et al., 2016; Table S7), and the resulting fragment was *in vitro* transcribed using the mMESSAGE mMACHINE T7 kit (Thermo Fisher Scientific).

Pairs of single guide RNAs (sgRNAs) were designed to target sites flanking each of the enhancers to be deleted (target site sequences listed in Table S7). sgRNAs were designed to have minimal possible off-target positions and were constructed using 60-mer oligos (Integrated DNA Technologies, Table S7) and a gRNA cloning vector (Addgene plasmid 41824; Mali et al., 2013) according to a publicly available protocol (https://media.addgene.org/cms/files/hCRISPR_gRNA_Synthesis.pdf). Complete sgRNA sequences were amplified from the cloning vector using primers listed in Table S7, and the resulting DNA fragments were *in vitro* transcribed using the MEGAshortscript T7 kit (Thermo Fisher Scientific). Cas9 mRNA and transcribed sgRNAs were purified using the MEGAclear kit (Thermo Fisher Scientific). Single stranded donor oligos (IDT, Table S7) were used to encourage homology driven repair to generate multiple F0 mice with identical deletion events for all enhancer deletions except hs123.

Cas9 mRNA (100 ng/μL final concentration), two sgRNAs (25 ng/μL final concentration each), and donor oligo (200 ng/μL) were mixed in microinjection buffer (10mM Tris, 0.1mM EDTA, pH 7.5), and the resulting mixture was injected into the cytoplasm of E0.5 FVB strain mouse embryos using standard procedures. All single enhancer knockouts were generated using fertilized eggs from wild-type FVB mice. Double enhancer knockouts were generated iteratively, using fertilized eggs harboring one of the deletions and delivering sgRNAs to target the other. Deletion events were identified by genotyping (primers listed in Table S7), and breakpoints were confirmed with Sanger sequencing. Details for founder mouse lines used are listed in Table S3. Founder lines were expanded and maintained by outcrossing mutation carriers with wild-type FVB animals to minimize the likelihood of a line harboring an off-target mutation.

RNA-Seq for Enhancer Knockouts

Individual forebrains were microdissected from E11.5 embryos by an experimenter blinded to the embryos' genotypes. Genotyping and gender determination for embryos were carried out using primers listed in Table S7. Samples were chosen for RNA-Seq such that a wild-type littermate was sequenced for each enhancer knockout embryo sequenced. Because the enhancers reside on the X chromosome, only male embryos were used for RNA-Seq. RNA was isolated using the RNAqueous Total RNA Isolation Kit (Thermo Fisher Scientific). RNA samples were DNase-treated with the TURBO DNA-free Kit (Thermo Fisher Scientific), and RNA quality was then assessed using a 2100 Bioanalyzer (Agilent) with an RNA 6000 Nano Kit. RNA sequencing libraries were made using the TruSeq Stranded mRNA Sample Prep Kit (Illumina). RNA-Seq libraries were subjected to an additional purification step using Agencourt AMPure XP beads (Beckman Coulter) to remove remaining high molecular weight products (Dickel et al., 2016). RNA-Seq library quality and concentration were assessed using a 2100 Bioanalyzer with the High Sensitivity DNA Kit (Agilent) and a Qubit Fluorometer with the Qubit dsDNA HS Assay Kit (Thermo Fisher Scientific). RNA-Seq libraries were sequenced with single end 50 bp reads on a HiSeq 2500 or 4000 (Illumina) at the Vincent J. Coates Genomics Sequencing Laboratory at UC Berkeley. To eliminate batch variation effects, all knockout and wild-type embryos for a given line were processed in the same batch, and the resulting barcoded libraries were pooled together for sequencing on the same flow-cell lane. RNA-Seq analysis was carried out as previously described (Dickel et al., 2016). Briefly, filtering and mapping were performed using Illumina-provided software, along with cutadapt_v1.1 (Martin, 2011), TopHat v2.0.6 (Trapnell et al., 2009), and HTSeq (Anders et al., 2015). For each sample, between 35 and 58 million usable reads remained following quality filtering. Differential gene expression analysis was performed with edgeR (Robinson et al., 2010) and excluded genes with very low expression values, defined by Cufflinks v2.2.1 (Trapnell et al., 2010) as having a fragment per kilobase of transcript per million mapped reads (FPKM) less than 1. For differential gene expression analysis, the *P*-values reported in figures are those prior to false discovery rate (FDR) correction, and the *P*-values following genome-wide FDR correction for the double enhancer deletion lines are reported in Table S5.

In situ Hybridization

Isolated embryonic brains (E12.5 or E13.5) used for *in situ* hybridization (ISH) were fixed overnight in 4% paraformaldehyde (PFA), transferred to 15% sucrose overnight followed by 30% sucrose overnight for cryoprotection, and then embedded and frozen in OCT compound for cryosectioning. Cryostat sections were cut coronally at 20 μm thickness. For *in situ* hybridization a rostro-caudal series of at least ten sections were examined. Section ISHs were performed using previously published digoxigenin-labeled riboprobes as previously described using RNase-free reagents and solutions (Stanco et al., 2014). Briefly, sections were washed in PBS, steamed in 10mM sodium citrate (pH = 6), washed in PBS then acetylated for 10 minutes (1.3% Triethanolamine, 0.06% HCl, 0.38% acetic anhydride). The sections were then prehybridized for 30 mins at 65°C (in a solution of 50% formamide, 50ug/mL heparin, 50ug/mL yeast tRNA, 5xSSC and 1%SDS) and then hybridized with DIG-labeled riboprobes overnight at 65°C. Sections were then washed in 5xSSC (pH 4.5) for 5 minutes at room temperature then washed twice in 0.2X SSC at 72°C for 30 minutes. After a 5 minute wash in NTT (0.15M NaCL, 0.1M Tris pH 8, 0.1% Tween), sections were blocked in 5% heat inactivated sheep serum in 2% blocking reagent in NTT for 1 hour at room temperature. Sections were then incubated overnight in anti-Digoxigenin-AP antibody, and following three washes in NTTML (0.15M NaCL, 0.1M Tris pH 9.5, 0.1% Tween, 50mM $MgCl_2$, 2mM Levamisole), the signal was revealed using BM purple at 37°C. Sections were then fixed in 4% paraformaldehyde and coverslipped.

The *Arx* probe was designed against exon 5 and 6 (chrX: 9054137-90543401 in mm9), linearized with PstI, and transcribed with a DIG labeling mix using the T3 polymerase (Roche). The probe was purified using an RNA clean and concentrator kit (Zymo Research).

Body Weight Measurements

Hemizygous null males used for body weight analyses were selected based on availability. For all lines, controls were the available wild-type male littermates of the hemizygous null males analyzed. Mice were weighed using a standard electronic laboratory scale. Measurements were taken weekly beginning at weaning, with each animal being weighed on a consistent day of the week from week to week, by a handler un-blinded to genotype.

Sample Selection for Neurological Phenotyping

Because the *Arx* locus resides on the X chromosome, phenotyping was performed only on male mice. All animals used for neurological phenotyping ranged from generation F2 to F4. With the exception of two of the hs119 deletion animals and one wild-type control, all animals phenotyped resulted from at least two generations of out crossing to wild-type to minimize possible off-target effects. For the dorsal forebrain enhancer knockouts (hs122, hs123, hs122/hs123), animals were selected using a matched littermate strategy. For each knockout animal phenotyped, a wild-type male littermate was phenotyped as a control. For the ventral forebrain enhancer knockouts (hs119, hs121, hs119/hs121), the four wild-type controls were littermates of at least one of the knockout animals phenotyped. Details for animals phenotyped are provided in Table S6.

Brain Sectioning and Immunohistochemistry

Postnatal animals were anesthetized with intraperitoneal avertin (0.015 ml/g of a 2.5% solution) and perfused transcardially with PBS and then with 4% paraformaldehyde (PFA). Whole brain was isolated and then subjected to 4-5 hours fixation in 4% PFA, cryoprotection in 30% sucrose in PBS, and cut frozen coronally on a freezing sliding microtome at 40 μm. For immunohistochemistry

all primary and secondary antibodies were diluted in PBS containing 10% Normal Serum, 0.25% Triton X-100 and 2% BSA. The following primary antibodies were used: rabbit anti-parvalbumin (1:3,000, Swant Swiss Abs), rat anti-somatostatin (1:200, Millipore), goat anti-somatostatin (1:100, Santa Cruz), mouse anti-calretinin (1:1,000, Millipore), rabbit anti-VIP (1:300, Immunostar) and goat anti-ChAT (1:100, Millipore). Sections processed for immunofluorescence were counterstained with Hoechst 33342 (Thermo Fisher Scientific). For indirect immunohistochemistry, sections were incubated with biotinylated secondary antibodies (Jackson), diluted 1:300, and processed by the ABC histochemical method (Vector Laboratories). Black reaction, to enhance contrast, was obtained by mixing 0.05% diaminobenzidine (DAB) plus 2.5% in a volume of 1% Cobalt chloride and 1% nickel ammonium sulfate. The reaction was carried out by adding 0.01% hydrogen peroxide (Adams, 1981).

Image Acquisition and Analysis

Brightfield images were taken using a Coolsnap camera (Photometrics) mounted on a Nikon Eclipse 80i microscope using NIS Elements acquisition software (Nikon). Brightness and contrast were adjusted and images merged using Photoshop or ImageJ software (Schneider et al., 2012).

Cell Counting

For assessing cell density in the postnatal neocortex on brightfield sections, 10x images were taken of the somatosensory cortex, encompassing all neocortical layers, from both hemispheres for each replicate. Images were opened with ImageJ (Schneider et al., 2012) to delimit and measure the region of interest (ROI). All cells in the ROI were counted by an investigator blinded to the animal's genotype. Cell counts were divided by the ROI area to determine cell density. Statistical analyses for cell counting were done with SPSS Statistics v15 software (SPSS Inc.). The statistical significance of multiple comparisons on continuous data was performed using the ANOVA test with a Tukey HSD or Scheffe posthoc to determine the significance between groups after checking that the data fit to a normal distribution (assessed by Shapiro-Wilk normality test) and that the variances were equal (determined by Levene's test). PV, VIP, and ChAT-expressing neuron populations are stable in wild-type animals during the postnatal stages examined (del Río et al., 1994; Gould et al., 1991; Taniguchi et al., 2011).

Hippocampal Measurements

Brain sectioning and image acquisition were performed as described above. For this analysis, sections were stained with DAPI. Measures of dentate gyrus length were obtained using ImageJ by tracing the total length of the superior and inferior blades of the gyrus on serial sections of right and left hippocampi following the appearance of the superior limb of the dentate gyrus. The total length of the *Cornu Ammonis* (CA) was measured similarly. Surface area measures of the dentate gyrus were performed for the whole dentate gyrus and restricted to the granule cell layer. Measures in figures are presented normalized to the length or area of age-matched wild-type littermates, with raw measurements provided in Table S6. Measurements were performed blinded to genotype.

QUANTIFICATION AND STATISTICAL ANALYSIS

Details regarding specific quantification and statistical analyses are provided throughout the main text and figures and in the METHOD DETAILS section above. Unless otherwise indicated, statistical analyses and plot generation were performed using R (www.r-project.org).

DATA AND SOFTWARE AVAILABILITY

The accession number for the RNA-seq data reported in this paper is GEO: GSE100394. No software was generated for this project.

Cell

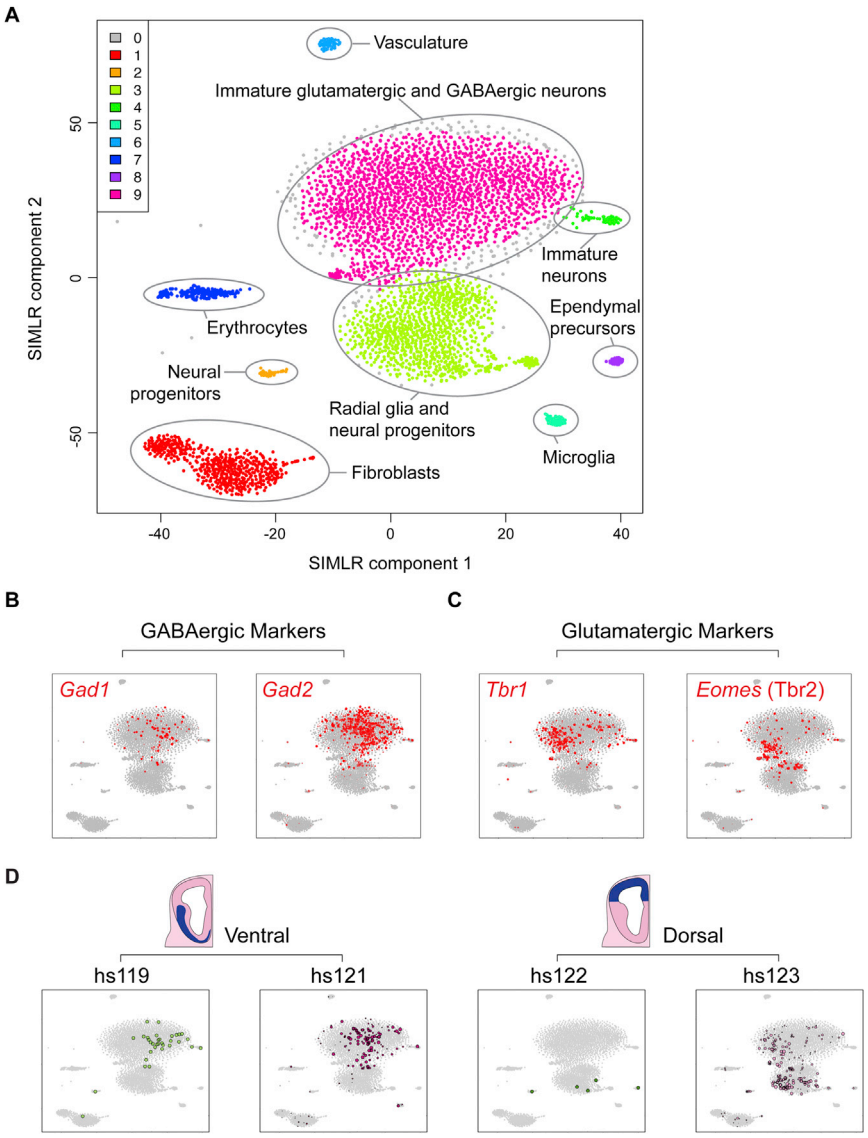

Figure S1. Single-Cell RNA-Seq Results for Transgenic E12.5 Forebrain, Related to Figure 2

Drop-Seq was performed on E12.5 forebrain from transgenic embryos harboring a fluorescent reporter gene under the control of one of the ultraconserved enhancers. This was done separately for each of the four enhancers.

(A) Cell-type clustering analysis for 4,723 single cell expression profiles captured across all Drop-Seq experiments (see Table S1). Each point indicates a unique single cell, and cells were clustered according to the similarity of their expression profiles (see STAR Methods). Cell type names for each cluster were determined based on the collection of marker genes identified for each cluster and the enriched gene ontology categories for these genes (Table S2).

(B and C) Same plots as (A), now showing the cells expressing markers of GABAergic (B) or glutamatergic (C) neuron identities highlighted in red.

(D) Cells expressing the fluorescent reporter gene under the control of one of the ultraconserved enhancers (green and pink dots). This is the same information as Figure 2C, except with reporter gene expressing cells labeled for one enhancer per plot.

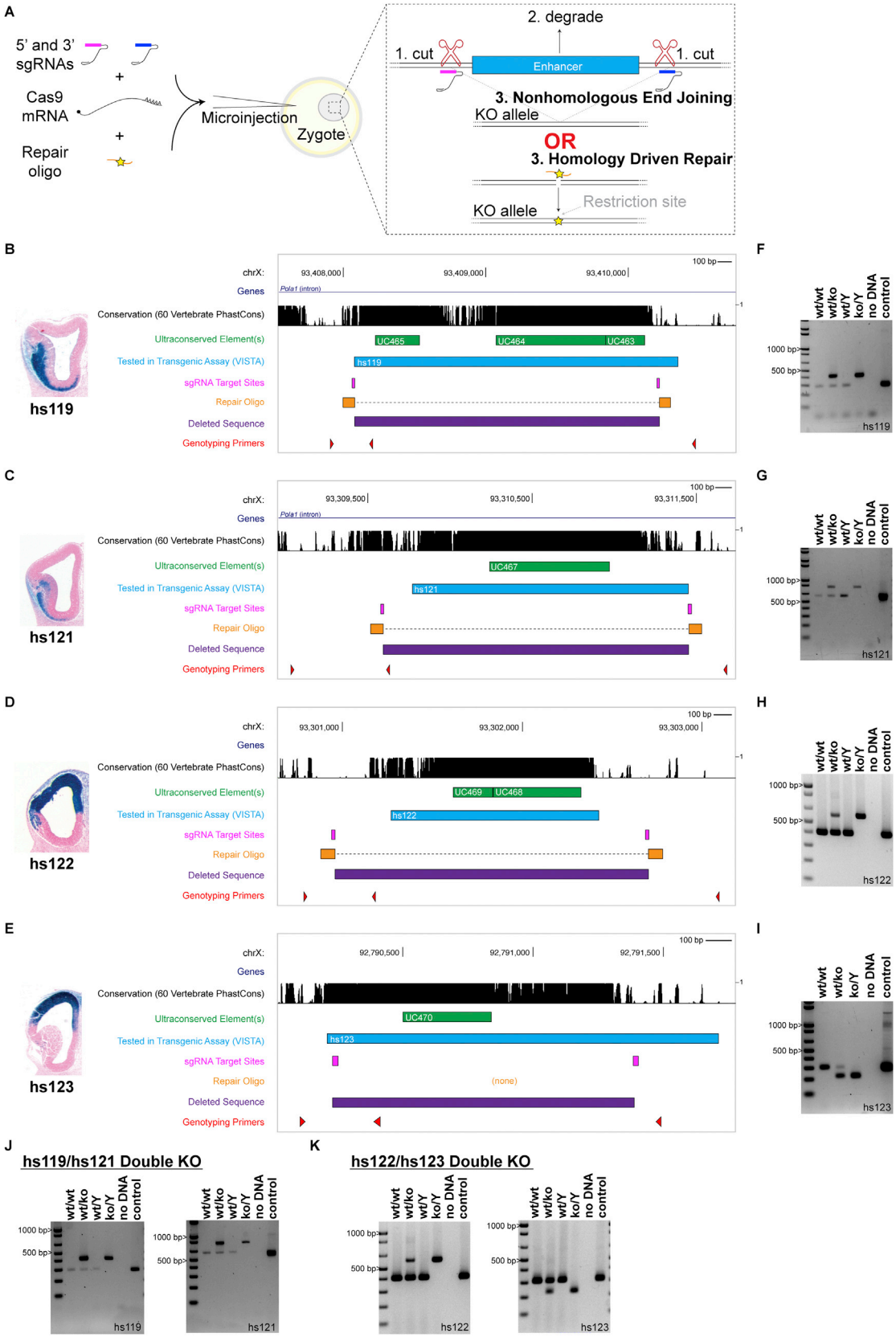

(legend on next page)

Figure S2. Cas9-Generated *Arx* Enhancer Knockout Mice, Related to Figure 3

(A) Overview of *in vivo* CRISPR/Cas9 editing methods used to generate enhancer knockout mice. Cas9 mRNA and two sgRNAs targeting sites flanking the enhancer were injected into single-cell mouse embryos. With the exception of hs123, a single-stranded homology oligo was also injected to attempt to generate independent founder lines with identical deletion events through homology driven repair (HDR). HDR-generated alleles were identified by the presence of a restriction site encoded in the repair oligo.

(B–E) Diagrams showing the genomic locations of (i) ultraconserved elements (green; from Bejerano et al., 2004); (ii) sequence tested in transgenic assays (blue; from Pennacchio et al., 2006; Visel et al., 2013; and https://enhancer.lbl.gov); (iii) the sgRNA target sites (magenta); (iv) the repair oligo (orange), (v) the sequence deleted (purple), and (vi) genotyping primers for each targeted enhancer (red arrowheads). sgRNA target sites and oligo sequences provided in Table S7.

(F–K) Genotyping to confirm enhancer deletions. Gel images showing genotyping results from wild-type (wt) and enhancer deletion (ko) mice for each single enhancer (F–I) or double enhancer (J and K) deletion generated. All *Arx* enhancers targeted reside on the X chromosome, so males are indicated by the presence of a Y chromosome (Y). Genomic coordinates for each deletion and additional details for each line generated are provided in Table S3.

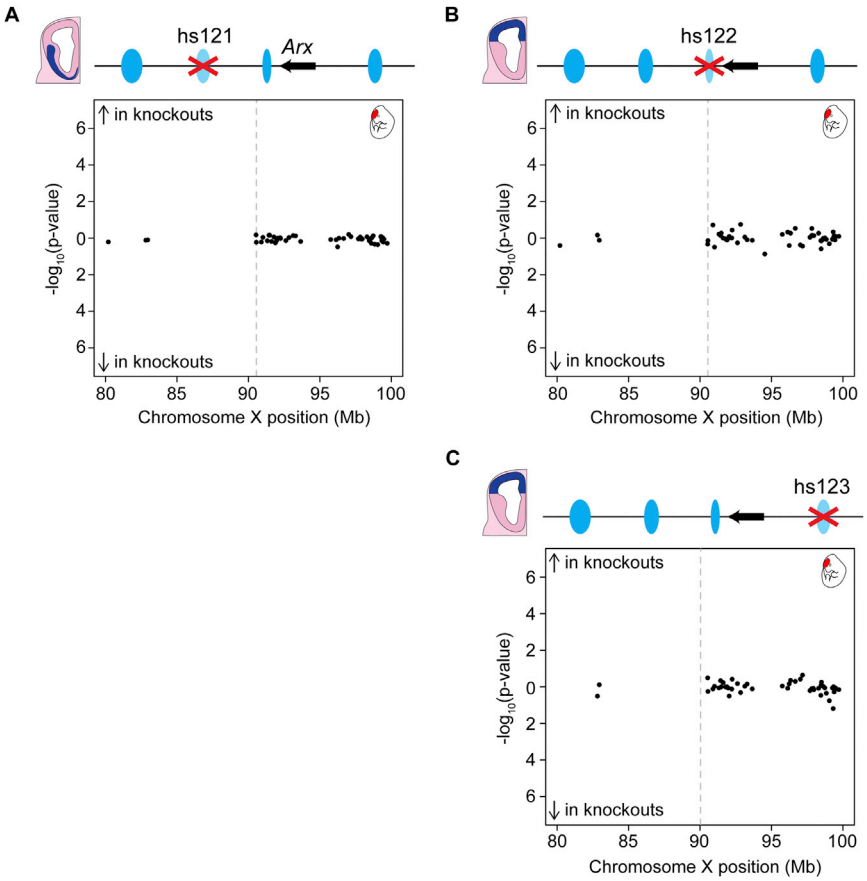

Figure S3. Gene Expression Changes Near Enhancers for Single Knockout Lines, Related to Figure 4

(A–C) RNA-Seq was performed on E11.5 whole forebrain from hemizygous male wild-type (n = 2) and hemizygous male knockout (n = 2) embryos from each single enhancer knockout line: A) hs121, B) hs122, C) hs123. p values indicate the statistical support for the difference between wild-type and knockout samples, and these were calculated by edgeR (Robinson et al., 2010). Points indicate individual genes, with results from all expressed genes within a 20 megabase (Mb) window around *Arx* shown. Gray dashed line indicates the position of the deleted enhancer.

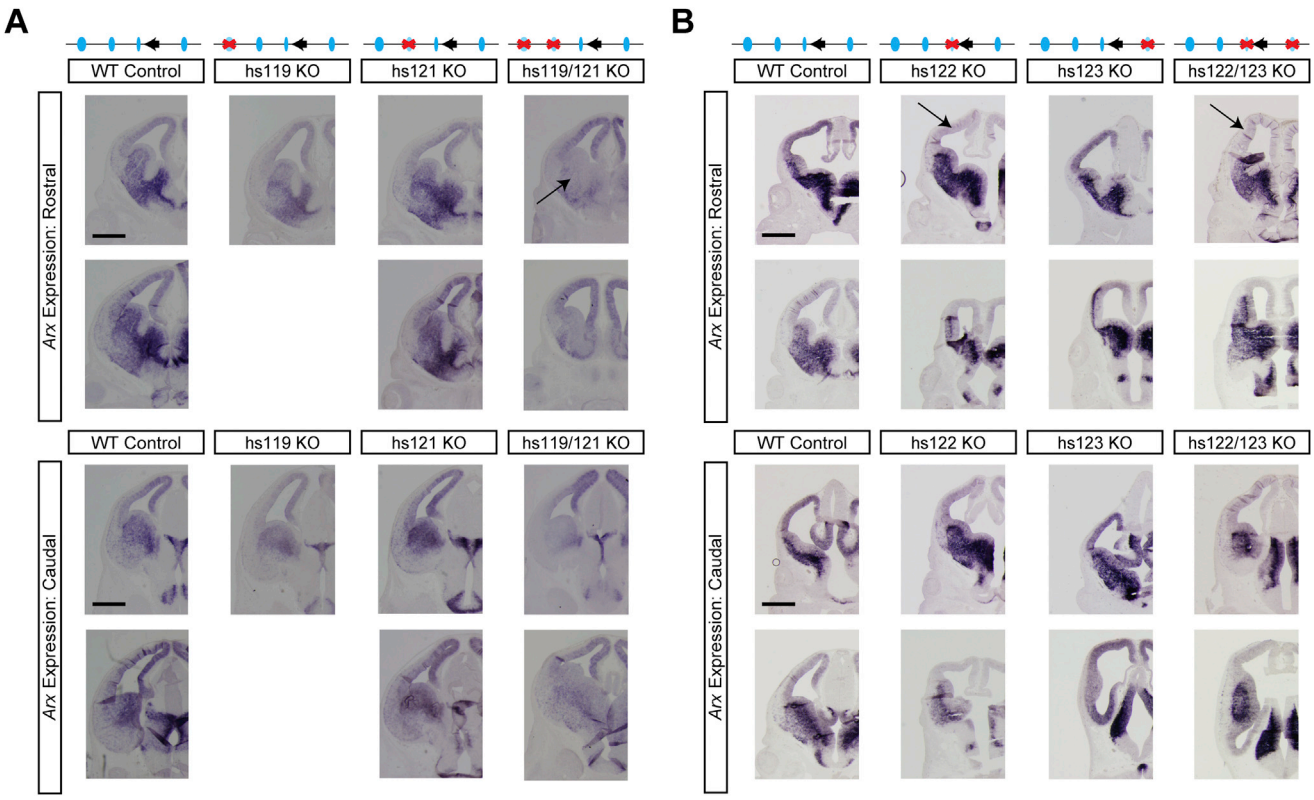

Figure S4. Biological Replicates for *In Situ* Hybridization of *Arx* Expression, Related to Figure 4

(A and B) *Arx in situ* was performed on coronal brain cross sections from embryos wild-type (WT) or hemizygous-null (KO) for the ventral (A) or dorsal (B) telencephalon enhancers. Shown are up to two biological replicates per genotype, in addition to those embryos shown in Figure 4. *Arx* expression is indicated by blue staining. Embryos are ages E13.5 (A) or E12.5 (B). Scale bars, 500 μm.

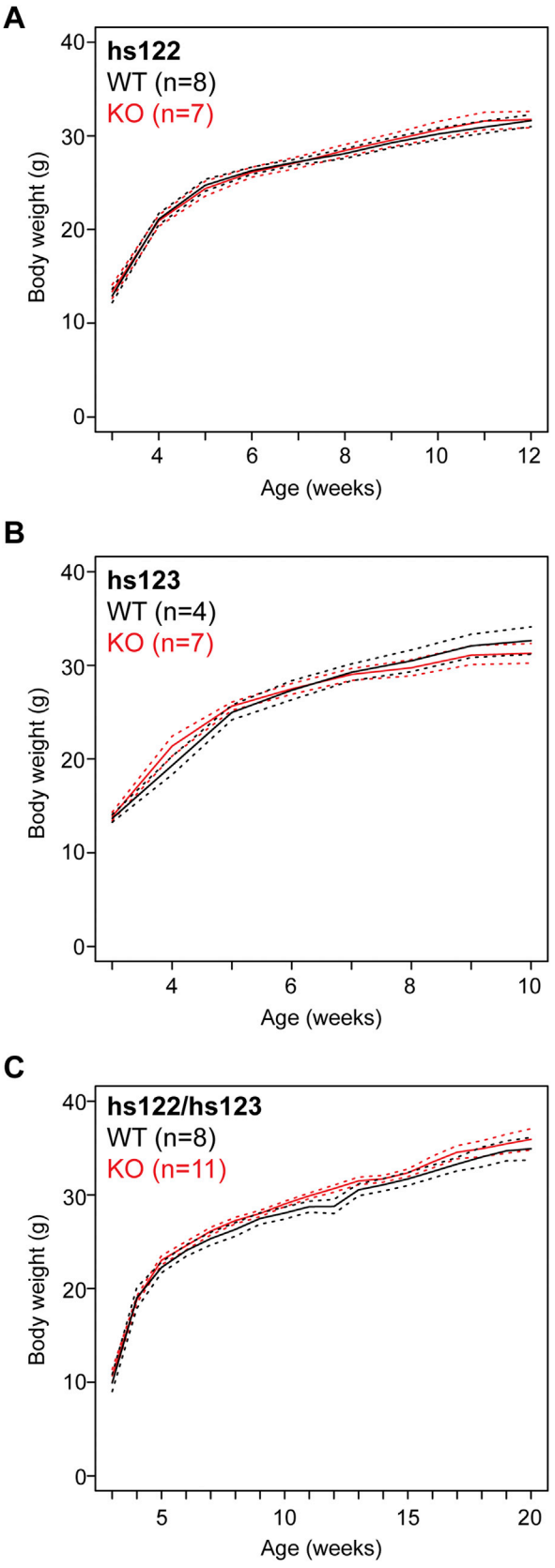

(legend on next page)

Figure S5. Weight Curves for Enhancer Deletion Mice, Related to Figure 5

(A–C) Mean (solid line) body weights for hemizygous-null male mice (KO, red) and wild-type male littermates (WT, black) for each single (A and B) or double (C) deletion of enhancers active in the dorsal forebrain. Mice were weighed weekly from weaning (3 weeks) up to 20 weeks of age. Sample sizes for each cohort are indicated on each plot, and dashed lines indicate standard error of the mean (SEM). No significant growth abnormalities were observed for dorsal forebrain enhancer deletions.

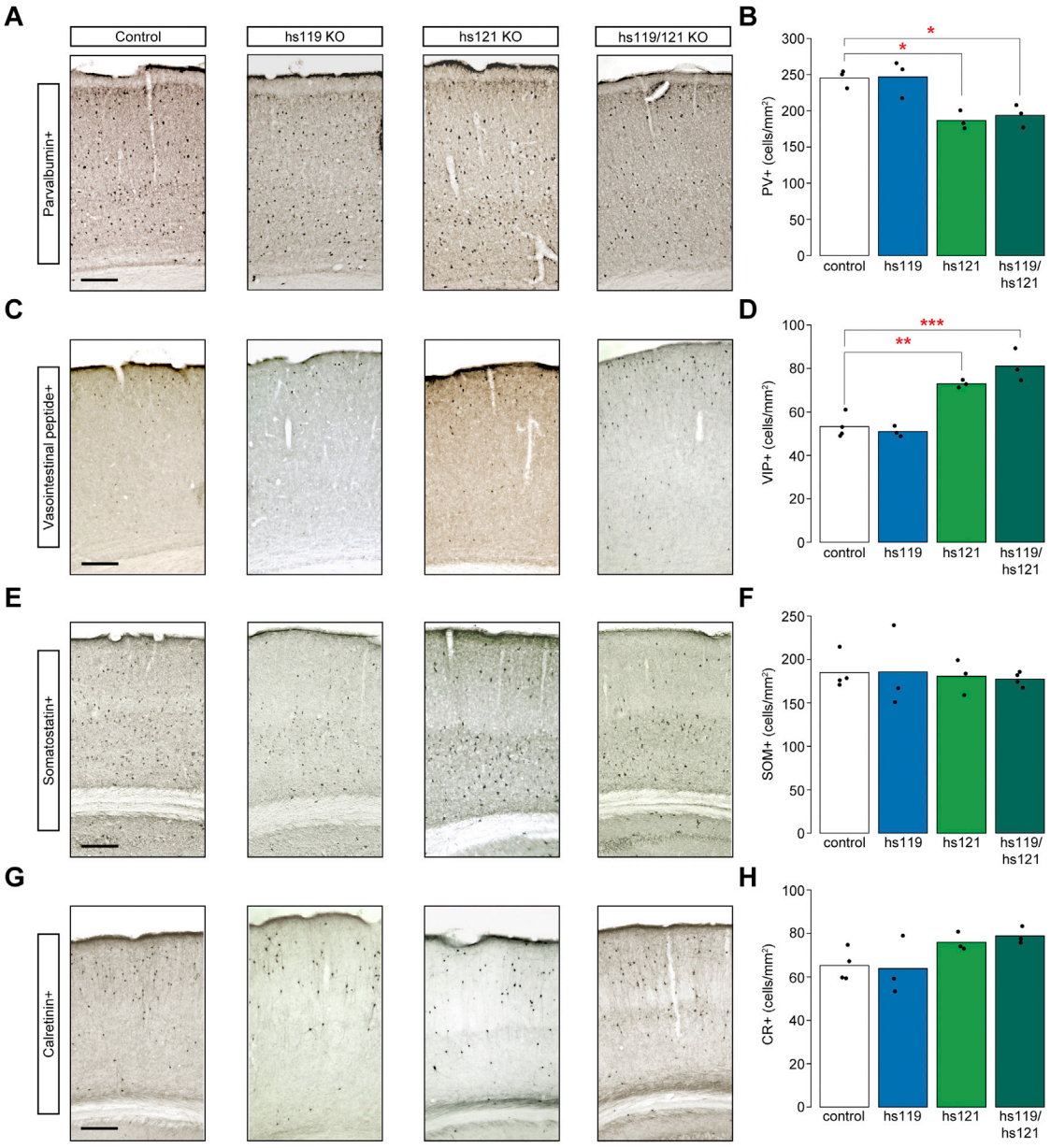

Figure S6. Loss of Ventral *Arx* Enhancers Results in Alterations in Interneuron Population Densities, Related to Figure 5

(A,C,E, and G) Representative images of coronal sections through the cortex of postnatal male wild-type (WT) and hemizygous enhancer deletion (KO) animals labeled via immunohistochemistry (black dots) for parvalbumin (A), vasointestinal peptide (C), somatostatin (E), and calretinin (G). Scale bar, 200 μm.

(B, D, F, and H) Bar graphs showing quantification of the density of neurons positive for parvalbumin (B), vasointestinal peptide (D), somatostatin (F), and calretinin (H). Bars indicate mean density, and dots indicate individual biological replicates. * $p < 0.05$, ** $p < 0.01$, *** $p < 0.001$. p values by ANOVA (see STAR Methods). Detailed information, including neuron counts and ages for each biological replicate, is provided in Table S6.

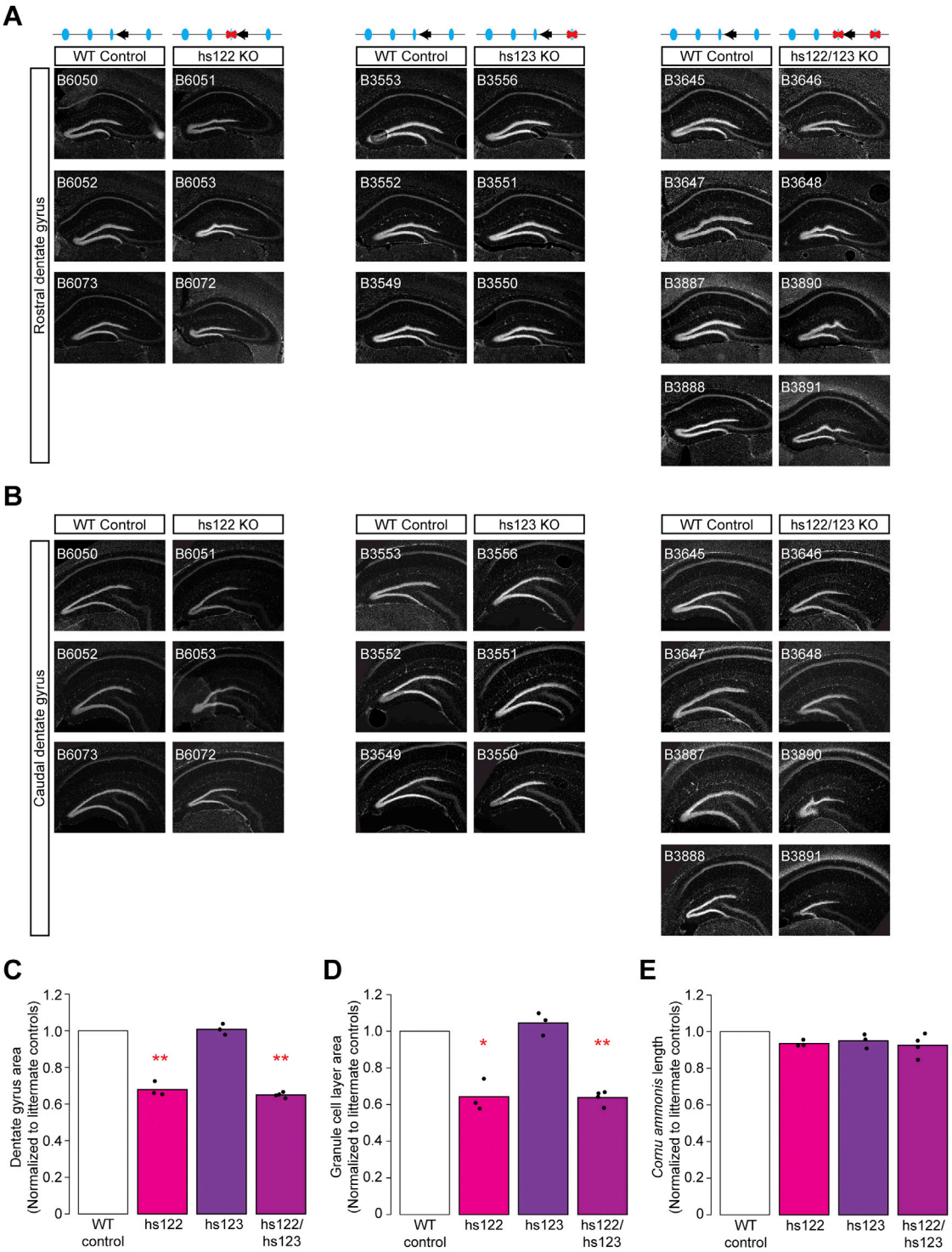

Figure S7. Dentate Gyrus Abnormalities Resulting from Loss of Dorsal *Arx* Enhancers, Related to Figure 6

(A and B) Shown are rostral (A) and caudal (B) coronal cross-sections of postnatal male mouse brains showing the dentate gyrus for all animals examined. Images of matched wild-type control (WT) and knockout (KO) littermates are shown side-by-side for comparison. The number in the top left of each image is the unique identifier for that sample (sample details provided in Table S6).

(C–E) Quantitative measurements of the whole dentate gyrus area (C), the dentate gyrus granule cell layer area (D), and Cornu Ammonis length (E) for all dorsal enhancer knockouts (values normalized to wild-type littermates). Bars show mean values for each enhancer deletion genotype, with individual biological replicates shown as points. Raw measurements for each animal (KO or control) provided in Table S6. *, $p < 0.05$; **, $p < 0.01$; two-tailed t test.